Bond-order and charge-density waves in the isotropic interacting two-dimensional quarter-filled band and the insulating state proximate to organic superconductivity

S. Mazumdar[1], R. T. Clay[1,2], and D. K. Campbell[3]
[1] *Department of Physics, University of Arizona, Tucson, AZ 85721*
[2] *Cooperative Excitation Project ERATO, Japan Science and Technology Corporation (JST)*
[3] *Department of Physics, University of Illinois , Urbana, Illinois 61801*
(February 1, 2008)

We report three surprising results regarding the nature of the spatial broken symmetries in the two-dimensional (2D), quarter-filled band with strong electron-electron interactions that provides a microscopic model of the 2:1 cationic organic charge transfer solids (CTS). First, in direct contradiction to the predictions of one-electron theory, we find a coexisting "bond-order and charge-density wave" (BCDW) insulating ground state in the 2D rectangular lattice for *all* anisotropies, including the isotropic limit. Second, in contrast to the interacting half-filled band, which exhibits one singlet-to-antiferromagnet (AFM) transition as the interchain coupling is increased from zero, there occur in the interacting quarter-filled band two distinct transitions: a similar singlet-to-antiferromagnet/spin-density wave (AFM/SDW) transition at small interchain coupling, giving rise to a bond-charge-spin density wave (BCSDW) state, followed by a second AFM/SDW-to-singlet transition at large interchain coupling. Third, we show that our conclusions remain unchanged if one assumes the conventional "effective 1/2-filled" lattice of dimer sites for the CTS: the dimer lattice unconditionally dimerizes again to give the same BCDW found in the quarter-filled band. We make detailed comparisons to recent experiments in the tetramethyl-tetrathiafulvalene (TMTTF), tetramethyl-tetraselenafulvalene (TMTSF), bisethylenedithio-tetrathiafulvalene (BEDT-TTF) and bisethylenedithio-tetraselenafulvalene (BETS)-based CTS. Our theory explains the mixed charge-spin density waves observed in TMTSF and certain BEDT-TTF systems, as well as the absence of antiferromagnetism in the BETS-based systems. An important consequence of this work is the suggestion that organic superconductivity is related to the proximate Coulomb-induced BCDW, with the SDW that coexists for large anisotropies being also a consequence of the BCDW, rather than the driver of superconductivity. We point out that the BCDW and BCSDW states are analogous to four different classes of "paired" semiconductors that are obtained within certain models of exotic superconductivity. That all four of these models can in principle give rise to superconductivity in the weakly incommensurate regime provides further motivation for the notion that the BCDW may be driving the superconductivity in the organics.

I. INTRODUCTION

Theoretical discussions of spatial broken symmetries in strongly correlated electron systems have largely focused on the 1/2-filled band Mott-Hubbard semiconductor. The one-dimensional (1D) case has been widely discussed in the context of polyacetylene[1,2]. Here it is known that Coulomb electron-electron (e-e) interactions can strongly enhance the $2k_F$ (k_F = one-electron Fermi wavevector) bond-alternation expected within the Peierls purely electron-phonon (e-ph) coupled model, giving rise to a periodic modulation of the bond-order, a bond-order wave (BOW). In the limit of very strong on-site Coulomb interaction, the BOW instability is usually referred to as the spin-Peierls (SP) instability. In the presence of intersite Coulomb interactions, and for certain relative values of the on-site and intersite interaction parameters, a charge-density wave (CDW), periodic modulation of the site charge density, can be the dominant instability[3]. The BOW and the CDW occur in largely nonoverlapping regions of the parameter space and compete against each other[3–6]. True antiferromagnetism (AFM)—ie, a long-range order (LRO) $2k_F$ spin-density wave (SDW)—is absent in for spin-rotationally invariant models in 1D, and the ground state is dominated by singlet spin coupling, which favors the BOW over the SDW. Two-dimensionality is thus essential for the SDW.

The 1/2-filled isotropic two-dimensional (2D) case has been investigated in great detail in recent years (mostly for the case of large intrasite Hubbard interaction but zero intersite interaction)[7], as this limiting case is known to describe the parent semiconductor compounds of copper-oxide based high temperature superconductors. The BOW instability that characterises the 1D chain is destabilized in 2D by Coulomb interaction[8–10], and the dominant broken symmetry here is the $2k_F$ SDW, with periodic modulation of the spin density. Most recently, it has been demonstrated that this SDW state appears for the smallest nonzero interchain hopping in weakly coupled 1/2-filled band chains[11], in agreement with previous renormalization group calculations[12,13]. As in 1D[6], there

is no CDW-SDW coexistence in 2D[8–10]. The absence of coexistence between the BOW and SDW for the 1/2-filled band in both 1D and 2D can be readily understood intuitively: the BOW requires spin-singlet coupling between alternate nearest neighbor spins, which clearly has to disappear in the SDW. An alternate way of viewing this is to observe that the probability of charge-transfer to the left and to the right in the AFM are exactly equal, and therefore the SDW cannot coexist with the BOW. On the other hand, both the BOW and the SDW require that the site-occupancies by electrons are strictly uniform, and thus neither the 1D BOW nor the 2D SDW will coexist with the CDW.

Coupled 1/2-filled band chains have also been discussed within the context of the so-called ladder systems[14]. Whether or not a given n-leg ladder system, for small n, exhibits the BOW now depends on whether n is odd or even. This feature of the ladder systems could have been anticipated from the physics of the odd versus even S Heisenberg chains[15]. Thus at least for the simplest monatomic lattices, ground states of the 1/2-filled band are known: the BOW, CDW and SDW phases compete against one another and do not coexist, and 2D behavior emerges for the smallest 2D coupling.

In contrast to the 1/2-filled band, broken symmetries in *non*-1/2-filled bands with strong e-e interactions have been investigated primarily in 1D limit[16–20] or at most in the quasi-1D regime of weak interchain coupling[21]. This emphasis likely arises from the theoretical preconception that finite one-electron hopping between chains destroys the nesting feature that characterizes the 1D limit, leading necessarily to the restoration of the metallic phase[22]. A recent work has examined coupled chains in the limit of weak e-e interactions[23]. The weak-coupling approximation employed in reference [23] reproduces the loss of nesting predicted within band theory. While the continuum renormalization group calculations[16,17] predicted CDW-SDW coexistence for *incommensurate* bandfillings, early quantum Monte Carlo calculations for the 1/4-filled band failed to find this coexistence[19]. Many more recent numerical simulations on discrete finite systems assume the absence of coexistence between the $2k_F$ BOW, the $2k_F$ CDW and the $2k_F$ SDW that characterizes that 1/2-filled band also applies to the non-1/2-filled bands. Indeed, it is often assumed that the CDW is driven by the e-ph interactions and the SDW by e-e interactions and that their effects are competing. This assumption is made despite the result mentioned above that already in the simplest case of the 1D 1/2-filled band, e-e and e-ph interaction effects are known not to be competing but to act in a co-operative way to give the enhanced $2k_F$ BOW[1].

Recently, we have begun a systematic study of the nature of the broken symmetry ground states in the 2D 1/4-filled band on an anisotropic rectangular lattice with both e-ph and e-e interactions[24,25]. Earlier work by us had already established the *cooperative* coexistence between the BOW and the period 4 "$2k_F$" CDW in the

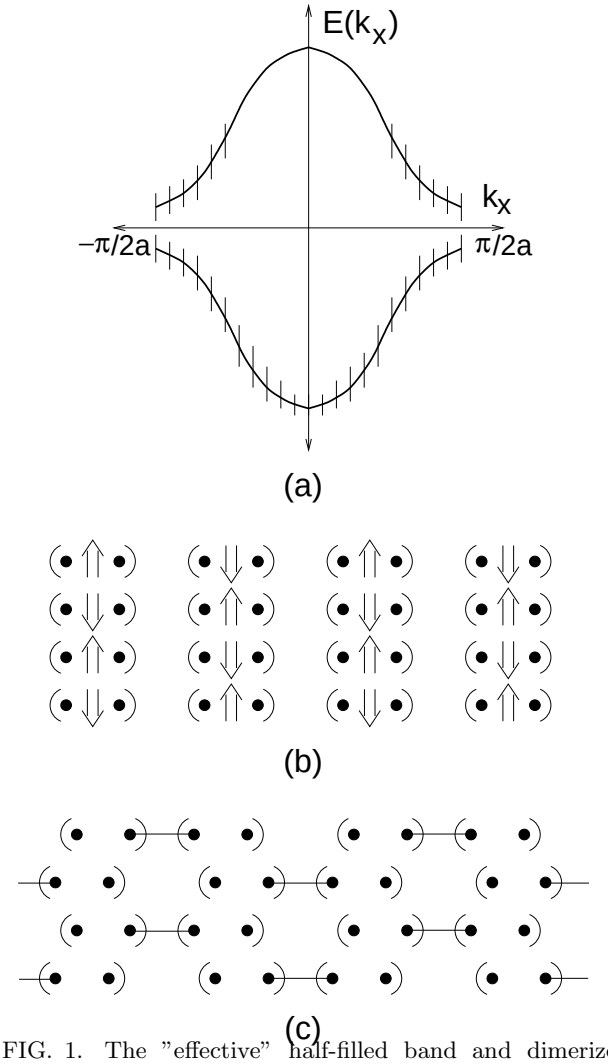

FIG. 1. The "effective" half-filled band and dimerized dimer model. (a) Dimerization in a 3/4-filled 1D band of *electrons* leads to a gap in the single particle spectrum at $k = \pm\pi/2a$ (a = lattice spacing), resulting in a half-filled upper subband. Note that although the actual CTS materials are indeed nominally 3/4-filled electron bands (hence 1/4-filled hole bands), in the text we follow the convention and refer to them simply as "1/4-filled". (b) A real space depiction of a 2D lattice of dimers in the strong correlation limit. The two sites within the parentheses form one lattice point of the dimer lattice, and the intradimer bonds are stronger than the interdimer bonds. The charge and spin populations on individual sites within each dimer are equal, and the effective 1/2-filled band lattice is antiferromagnetic in 2D. (c) Schematic of a frozen valence bond state resulting from the dimerization of dimer lattice. The interdimer bonds are now different; the line denotes a singlet bond. This frozen valence bond diagram is relevant in the 1D limit, and then again for the strongly 2D case, where the antiferromagnetism has disappeared. The antiferromagnetic phase that occurs for intermediate interchain coupling is shown in Fig. 2.

1D 1/4-filled band, with each broken symmetry enhancing the other, for both noninteracting[26] and interacting[27] electrons. The latter results have been sub-

sequently confirmed by Riera and Poilblanc[28]. In the more recent work[24,25] we have demonstrated an apparently unique feature of the 1/4-filled band: namely, the coexistence of the BOW-CDW with the period 4 "$2k_F$" SDW, giving rise to a coupled Bond-Charge-Spin density wave (BCSDW) that appears for weak interchain electron transfer between chains.

In the present paper, we extend our calculations to the full range of anisotropies, from uncoupled chains to an isotropic 2D lattice. We include both the SSH intersite phonons that drive a BOW[2] and the Holstein phonons that drive a CDW[29]. We list three primary motivations for this extension[25]. First, the cooperative coexistence between the BOW and the $2k_F$ SDW found in the 1/4-filled band for *weak* interchain transfer is exactly opposite to the competition between the $2k_F$ BOW and the $2k_F$ SDW (with the latter dominating for nonzero interchain transfer) in the 1/2-filled band. It is then immediately natural to ask what the nature of the ground state is for *strong* interchain hopping of electrons in the 1/4-filled band. Second, from a more general theoretical perspective, whether or not the vanishing of density waves that is predicted by one-electron nesting ideas remains true for strongly correlated electrons is of considerable general interest. Finally, our results are likely to have relevance to experimental observations in the organic CTS, including those that exhibit superconductivity[30–32].

Our investigations yield the surprising result that the coexisting Bond-Charge density wave (BCDW) persists as the ground state of the strongly correlated 1/4-filled band in 2D for *all* values of the interchain electron transfer, including the isotropic limit. We show that this result can be understood physically as a consequence of interchain confinement arising from strong intrachain Coulomb interactions[33–35]. The SDW component of the BCSDW, on the other hand, attains a maximum amplitude at some intermediate interchain transfer, after which it typically vanishes at a critical value of the transfer.

In order to discuss applications of results to real materials, including the 2:1 cationic CTS, we need to clarify an important aspect of our approach *vis-a-vis* most previous work on models of these materials. In our above discussion of band-filling, "1/4-filled" is defined in the usual manner: namely, in the absence of the BCDW, the lattice is uniform in at least one direction, and the average density of electrons *per site* is 1/2. In real materials, crystal structure effects often cause a lattice dimerization that is unrelated to any underlying electronic or magnetic instability (see below)[36]. As shown in Fig. 1(a), this dimerization leads to a gap in the single electron spectrum at $k_F = \pi/2a$, and consequently suggests using an effective 1/2-filled band model that focuses on the upper subband. In real space terms, this approximation amounts to considering the system as a set of (tightly bound) dimers (*i.e.*, a diatomic lattice) with one electron per *dimer* site, as shown in Figure. 1(b). This approach has been widely applied[36–40], particularly with considerable success in the context of the magnetic field-induced spin density wave (FISDW) in 2:1 salts of TMTSF[41,42]. As we show below, a further dimerization of the dimer lattice is unconditional in both 1D (the well-known spin-Peierls transition) and 2D (a surprising new result), and that this *dimerization of the dimer lattice leads spontaneously to different electronic populations on the sites within a dimer, i.e., to the same $2k_F$ CDW that occurs in the 1/4-filled (monoatomic) band* (see Fig. 1(c)). For small interchain electron transfer, the BCSDW will therefore have nearly the same structure as the original 1/4-filled band. This is a third new result, perhaps also surprising, and shows that the number of electrons per site within a unit cell is a more fundamental parameter than the bandfilling: the latter is strictly a one-electron concept of limited use in the interacting electron picture.

We expect our results to be relevant for the 1D semiconductors $(TMTTF)_2X$, the so-called "quasi-1D" organic superconductors $(TMTSF)_2X$, as well as the 2D organic superconductors (BEDT-TTF)$_2$X and the more recently synthesized $(BETS)_2X$[43]. In reference [24] we showed that the highly unusual "mixed CDW-SDW state"[36,44,45] found in $(TMTTF)_2Br$, $(TMTSF)_2PF_6$ and $(TMTSF)_2AsF_6$ can be explained naturally as the BCSDW state within the strongly correlated 1/4-filled band scenario. Our current work shows that dimerization of the dimer lattice leads to the same results, and hence the weak high temperature dimerization along the stack axis[36] is effectively irrelevant: starting from either the 1/4-filled model or the effective 1/2-filled scenario, the final outcome is the same[46].

With these comments complete, we can describe the organization of the remainder of the paper. In Section II we introduce our model Hamiltonian, as well as that of the dimerized dimer model. In Section III, we present physical, intuitive arguments, based on a configuration space picture of broken symmetry[3,8,20,27] that predict both the BCSDW for weak interchain electron transfer and the persistent BCDW state in the isotropic limit. In Section IV, we present the results of extensive numerical studies, exploring behavior in both the strict 1D limit and for the full range of anisotropies in the quasi-2D case. These studies, in confirmation of the qualitative predictions of Section III: (i) establish the persistence of the BCDW up to the isotropic limit; (ii) suggest the occurrence of two quantum critical transition as an SDW first appears for weak transverse hopping and then disappears for the nearly isotropic case; and (iii) prove the equivalence of the 1/2-filled dimerized dimer and 1/4-filled monatomic lattices. For clarity, in Section V we summarize our theoretical conclusions; readers not interested in the underlying physical arguments or numerical details can skip directly to this summary in Section V. In Section VI, we examine in some detail several recent experiments that indicate the applicability of our theory to the insulating states that are observed to be proximate to the superconducting states in the organic CTS. Finally, in Section VII, we indicate possible future di-

rections for our research, focusing on commensurability defects in the BCDW state and their possible role in the proximate superconducting phases. We point out several intriguing similarities between this potential microscopic mechanism for superconductivity and other recent phenomenological models. We conclude the article with three appendices, which deal with various more technical arguments and details of the numerical methods.

II. MODELS AND OBSERVABLES

We consider two different extended Peierls-Hubbard Hamiltonians on a rectangular lattice 2D with (in general) anisotropic electron hopping. The first model describes a monatomic 1/4-filled band and is defined by the Hamiltonian

$$H = H_0 + H_{ee} + H_{inter} \tag{1a}$$

$$H_0 = -\sum_{j,M,\sigma}[t-\alpha(\Delta_{j,M})]B_{j,j+1,M,M,\sigma} + \beta\sum_{j,M} v_{j,M}n_{j,M}$$

$$+K_1/2\sum_{j,M}(\Delta_{j,M})^2 + K_2/2\sum_{j,M}v_{j,M}^2 \tag{1b}$$

$$H_{ee} = U\sum_{j,M} n_{j,M,\uparrow}n_{j,M,\downarrow} + V\sum_{j,M} n_{j,M}n_{j+1,M} \tag{1c}$$

$$H_{inter} = -t_\perp \sum_{j,M,\sigma} B_{j,j,M,M+1,\sigma} \tag{1d}$$

In the above, j is a site index, M is a chain index, σ is spin, and we assume a rectangular lattice[24,25,47]. As $t_\perp$ varies from 0 to t, the electronic properties vary from 1D to 2D. An implicit parameter in the above Hamiltonian is the bandfilling, or more precisely ρ. We shall focus on the 1/4-filled case, for which $\rho = 1/2$. In applications to the organic CTS, each site is occupied by a single organic molecule, the displacement of which from equilibrium is described by $u_{j,M}$ (with $\Delta_{j,M} = (u_{j+1,M} - u_{j,M})$); $v_{j,M}$ is an intra-molecular vibration, $n_{j,M,\sigma} = c^\dagger_{j,M,\sigma}c_{j,M,\sigma}$, $n_{j,M} = \sum_\sigma n_{j,M,\sigma}$, and $B_{j,k,L,M,\sigma} \equiv [c^\dagger_{j,L,\sigma}c_{k,M,\sigma} + h.c.]$, where $c^\dagger_{j,L,\sigma}$ is a Fermion operator. We treat the phonons in the adiabatic approximation and are interested in unconditional broken symmetry solutions that occur for e-ph couplings $(\alpha,\beta) \to 0^+$. All energies such as U, V, and $t_\perp$ will be given in units of the undistorted intrachain hopping integral t.

The second model describes a *diatomic/dimer* lattice, with one electron per dimer. The Hamiltonian for this case is similar to that above, with identical H_{ee} and H_{inter}, but with modified intrachain one-electron term H_0',

$$H_0' = -t_1\sum_{j,M,\sigma} B_{2j-1,2j,M,M,\sigma} \tag{2}$$
$$-\sum_{j,M,\sigma}[t_2 - \alpha\Delta_{j,M}]B_{2j,2j+1,M,M,\sigma} + \frac{K}{2}\sum_{j,M}(\Delta_{j,M})^2$$

In the above each pair of sites (2j–1,M) and (2j,M) forms a dimer with fixed hopping $t_1 > t$ between them, $\Delta_{j,M} = (u_{2j+1,M} - u_{2j,M})$, with $u_{2j-1,M} = u_{2j,M}$; this means that there is no modulation of the intradimer bond length, and the dimer unit is displaced as a whole. As written, the model assumes an "in-phase" 2D arrangement of the dimer units (*i.e.*, dimers on different chains lie directly above one another), which we have determined to be the lower energy configuration for both zero and nonzero $\Delta_{j,M}$. Notice that H_0' does not contain the Holstein on-site e-ph coupling. Nevertheless, we will show that a site-diagonal CDW is a consequence of the BOW here.

The broken symmetries we are interested in are (i) the BOW, with periodic modulations of the intrachain *nearest neighbor* bond order $\langle\sum_\sigma B_{j,j+1,M,M,\sigma}\rangle$; (ii) the CDW, with periodic modulations of the site charge-density $\langle n_{j,M}\rangle$; and (iii) the SDW, with periodic modulations of the site spin-density $\langle n_{j,M,\uparrow} - n_{j,M,\downarrow}\rangle$. Note that in case of the dimer lattice (Eq. (2)) we are interested in both intra- and interdimer charge and spin modulations, although bond modulations can occur only between dimers. Furthermore, in the CDW and the SDW the modulations of the site-based densities occur along both longitudinal and transverse directions (though not necessarily with the same periodicities, see below). In case of the BOW, a complete description would require the determination of the phase difference between consecutive chains.

III. CONFIGURATION SPACE PICTURE OF SPATIAL BROKEN SYMMETRY

The physical arguments presented in this section provide crucial insights that allow us to anticipate the apparently counterintuitive results of this paper. The need to develop such arguments arises from the limitations inherent in all true many-body numerical simulations of strong correlated electron systems: namely, one can study only systems of limited size and distinguishing finite-size artifacts from true results requires physical understanding. In turn, true many-body numerical methods are essential here because of the intermediate magnitude of the e-e interactions (comparable to the bandwidths) in the organic CTS, which renders both mean field and perturbation theoretic approaches questionable. For instance, even in the strictly 1D limit, where well-established RG[16] and bosonization[17] techniques have existed for decades, for the *intermediate* coupling regime, there have recently been some surprising discoveries in the phase diagram of the extended Hubbard model[48,49]. In 2D, developing a

clear physical intuition is still more crucial, as numerically tractable lattices are even farther from the thermodynamic limit, and the competition among broken symmetries is likely to be more subtle. Brief presentations of these physical ideas for $t_\perp = 0$[26,27] and $t_\perp << t$[24] have been made previously. Here we discuss these ideas for the complete range $0 \leq t_\perp \leq t$, focusing on (i) the transition from 1D to 2D, and (ii) the difference from the 1/2-filled band *monatomic* lattice.

A physical picture of spatial broken symmetry in strongly correlated electron systems must necessarily be based on configuration space ideas, as one-electron bands have simply ceased to exist for strong e-e interaction. Within the configuration space picture of broken symmetry[3,8,20], each broken symmetry state, independent of band-filling, can be associated with a small number of equivalent configurations that are related by the symmetry operator in question. For commensurate ρ, these configurations are easily determined by inspection. The relevant configurations consist of repeat units which themselves possess the same periodicity as the density wave. For illustration, we choose the 1D 1/2-filled band. In this case, each broken symmetry has two extreme configurations, the pairs corresponding to the SDW, BOW and CDW being, respectively: the two Néel states ... $\uparrow\downarrow\uparrow\downarrow$ ... and ... $\downarrow\uparrow\downarrow\uparrow$ ... (SDW); the two nearest neighbor valence bond diagrams (1,2)(3,4)(5,6)....(N – 1,N) and (N,1)(2,3)(4,5)....(N – 2, N – 1) (where (i,j) is a spin singlet bond between sites i and j and N is the number of sites) (BOW); and the configurations ...202020... and ...020202...(where the numbers denote site occupancies) (CDW). N applications of the one-electron hopping term in Eq. (1) on any one extreme configuration (corresponding to a given broken symmetry) generates the other extreme configuration, but for $N \rightarrow \infty$ this mixing of configurations is small, and the ground state resembles one or the other of the extreme configurations *qualitatively*, with reduced spin moment, bond order or charge-density difference due to quantum fluctuations[3].

The key insight of the configuration space heuristics is that the qualitative effects of many-body Coulomb interactions, as well as additional one-electron terms, can be deduced from their effects on any one of the extreme configurations[3,8,20]. As a trivial example of this, a repulsive Hubbard U destroys the CDW in the 1/2-filled band, simply because double occupancies in the extreme configuration ...202020... "cost" prohibitively high energy. Significantly, in the 1/2-filled band, the extreme configurations favoring the SDW, the BOW and the CDW are different, and there is a complete lack of overlap between them. This essentially guarantees the absence of coexistence among these broken symmetries in both 1D and 2D.

To apply these ideas to the 1D 1/4-filled band, we begin by considering the on-site charge configurations. A $2k_F$ ($4k_F$) density wave here has period 4 (2) in configuration space. As discussed above, the extreme configurations of interest must also have period 4 or 2, and there are then only three distinct sets of extreme charge configurations. These contain the repeat units ...2000..., ...1100..., and ...1010..., respectively, where the numbers again denote site occupancies. There are four distinct configurations for sets 1 (...2000...) and 2 (....1100....), whereas there are only 2 for set 3 (....1010....). By analogy with the 1/2-filled band (see above), we now introduce spins and note that configurations belonging to sets 2 and 3 can again have spin singlet bonds between pairs of nearest neighbor singly occupied sites, or the spins of the occupied sites can alternate as in the 1/2-filled band Néel configurations. Let us now show, by considering the different cases separately, how e-e interactions affect these configurations and how an understanding of these effects suggests (correctly!) the broken symmetries to be studied.

A. 1/4-filled band, $t_\perp = 0$, $U = V = 0$

The non-interacting case provides a simple example to introduce some of the important differences between the 1/4-filled and 1/2-filled bands. Actual calculation indicates that within the 1D Holstein model the charge densities ρ_j on the sites have the functional form[26]

$$\rho_j = 0.5 + \rho_0 \cos(2k_F ja) = 0.5 + \rho_0 \cos(\pi j/2) \qquad (3)$$

This charge density pattern could have been anticipated by focusing on the extreme configuration ...2000..., which also predicts three different charge densities (large, intermediate, small and intermediate), since each '0' that is immediately next to a '2' is different from the other pair of sites labeled '0' that are further away from the '2'. occupancy scheme ...2000..., the probabilities of charge-transfer between a '2' and the two neighboring '0's are larger than that between the two neighboring '0's themselves. For nonzero α in Eq. (1), this difference in charge-transfers leads to lattice distortion of the form

$$u_j = u_0 \cos(2k_F ja) = u_0 \cos(\pi j/2), \qquad (4)$$

with bonding pattern "SSWW" (for strong, strong, weak, weak), where a strong (weak) bond has hopping $t_S > t$ ($t_W < t$). This then is one very important difference from the 1/2-filled band: whereas in the 1/2-filled band differences in bond-orders arise from spin-effects only (the probability of charge-transfer is greater between nearest neighbor singlet-coupled sites than between nearest neighbor non-bonded sites[3]), in non-1/2-filled bands this difference can also originate from site occupancies. *Precisely because the BOW and the CDW here are both derived from the same extreme configuration,* they coexist in the noninteracting 1/4-filled band[26].

B. 1/4-filled band, $t_\perp = 0$, $U, V > 0$

For nonzero (positive) U and V, the interplay among the various possible broken symmetries becomes both

more subtle and more interesting. Since double occupancies "cost" energy, the extreme configuration ...2000... is suppressed even at a relatively small U[27]. For the strongly correlated ($U \rightarrow \infty$) 1D 1/4-filled band with convex long range interactions, Hubbard showed that there exist *two* different Wigner crystals, with occupancy schemes ...1100... and ...1010...[50]. At first glance, the extreme configuration ...1010..., corresponding to a period 2 "$4k_F$"CDW[50], appears to be strongly preferred, but in fact more careful analysis shows that it dominates the ground state only for fairly substantial V[51]. This can be seen rigorously for $U \rightarrow \infty$, where the 1/4-filled *spinful* band can be mapped rigorously to the 1/2-filled *spinless* band[52], which in turn can be mapped (via a Jordan-Wigner transformation) to an anisotropic Heisenberg spin 1/2 chain[53]. Using this approach, one finds that the period 2 "$4k_F$" CDW becomes the ground state only for $V > V_c = 2$ (in units of $|t|$)[54]. For finite U, numerical results[55] show that V_c is slightly larger than 2. Given the estimated values of V in the organic CTS, it seems unlikely that they will exhibit this (...1010...) intrachain ordering. This expectation is strongly supported by the result that the ...1010... CDW cannot coexist with the BOW[3–6], whereas the $(TMTTF)_2X$ are known to exhibit a low-temperature transition to a SP-BOW ground state[32].

For $V < V_c$ the extended 1D Hubbard model at 1/4-filling is a Luttinger liquid[56] that is also susceptible to a $2k_F$ bond and charge distortion, and it is this distortion that can be described by any one of the four equivalent configurations ...1100...[27]. The $2k_F$ CDW compatible with the ...1100... configuration has the form

$$\begin{aligned}\rho_c(j) &= 0.5 + \rho_0 \cos(2k_F ja - 3\pi/4) \\ &= 0.5 + \rho_0 \cos(\pi j/2 - 3\pi/4),\end{aligned} \tag{5}$$

This particular CDW also coexists with a BOW, since the charge-transfer across a '1 – 1' bond is different from that across a '1 – 0' (or '0 – 1') bond, which again is different from the charge-transfer across a '0 – 0' bond. It is a subtle but crucial fact, confirmed by earlier numerical studies[27], that this same CDW can now promote *two* different BOWs, each with three different bond strengths. In each of these the '0 - 0' bond is the weakest, but depending upon the strength of the Coulomb interaction, the '1 - 1' bond can be stronger than a '1 – 0' (or '0 – 1') bond (since charge-transfer in the former can occur in both directions), but it can also be weaker (since charge-transfer in the former leads to double occupancy, while no double occupancy is created in the charge transfer between a '1' and a '0'). Consistent with this and the numerical results[27], we shall refer to the first bonding pattern as "SUWU" (for a strong '1 – 1' bond, undistorted '1 –0' bond, weak '0 – 0' bond, followed by an undistorted '0 – 1' bond), where a strong bond has $t_S > t$, an undistorted bond has $t_U = t$, and a weak bond has $t_W < t$. This BOW has pure period 4 "$2k_F$" periodicity and is accompanied by lattice distortion

$$u_j = u_0 \cos(2k_F ja - \pi/4) = u_0 \cos(\pi j/2 - \pi/4). \tag{6}$$

Again consistent with the numerical results, we call the second bonding pattern "W′SWS" (for a stronger weak '1 – 1' bond, strong '1 – 0' bond, weak '0 – 0' bond and strong '0 – 1' bond, with $t_S > t > t_{W'} > t_W$). Interestingly, the W′SWS bonding pattern is a superposition of the pure $2k_F$ period 4 SUWU structure and the pure $4k_F$ period 2 SWSW structure and is accompanied by lattice distortion

$$\begin{aligned}u_j &= u_0[r_{2k_F} \cos(2k_F ja - \pi/4) + r_{4k_F} \cos(4k_F ja)] \\ &= u_0[r_{2k_F} \cos(\pi j/2 - \pi/4) + r_{4k_F} \cos(\pi j)],\end{aligned} \tag{7}$$

where r_{2k_F} and r_{4k_F} are the relative weights of the $2k_F$ and $4k_F$ bond distortions, respectively[27]. These results were established numerically in reference [27], where from comparisons to available experimental data in the 1:2 anionic TCNQ systems it was also shown that the phase relationship between the coexisting $2k_F$ CDW and the W′SWS BOW (the W′ bond connects sites with greater charge densities than the W bond) is precisely in agreement with theory.

Very importantly, we show below that the dimerization of the dimer lattice with one electron per dimer also leads to a W′SWS bonding pattern (see Fig. 1(c)), which in its turn promotes the site occupancy scheme ...1100.... This coexistence will therefore occur in either the full 1/4-filled band model or the effective 1/2-filled, dimerized dimer approach.

C. 1/4-filled band, $t_\perp << t$, $U, V \neq 0$.

The above two BOW-CDWs describe the ground state of the interacting 1/4-filled band in the limit of $t_\perp = 0$, where the '1 - 1' bond is a singlet. As in the 1/2-filled band though, singlets are expected to give way to SDW order for $t_\perp \neq 0$. Thus we must understand the role of the spin degrees of freedom. Once specific spins are assigned to the sites labeled '1' in the ...1100... configuration, the sites labeled '0' become distinguishable, as a given '0' site is now closer to one particular '1' (up or down) than the other[24]. In this case the '0' site is expected to acquire the spin characteristic of its neighboring '1'. The charge and spin along a chain can now thus be denoted as $\uparrow, \downarrow, _{\downarrow,\uparrow}$, where the sizes of the arrows are schematic measures of the charge and spin densities on the sites. Note that this represents the SDW of the form

$$\begin{aligned}\rho_s(j) &\equiv \langle c^\dagger_{j,M,\uparrow} c_{j,M,\uparrow} - c^\dagger_{j,M,\downarrow} c_{j,M,\downarrow} \rangle \\ &= \rho_{s2k_F} \cos(2k_F ja - \pi/4) + \rho_{s4k_F} \cos(4k_F ja - \pi),\end{aligned} \tag{8}$$

which *coexists* with the BOW and CDW.

Commensurability effects imply that the possible phase shifts between adjacent chains in the anisotropic 2D system are 0, $\pi/2$ and π, and we have performed

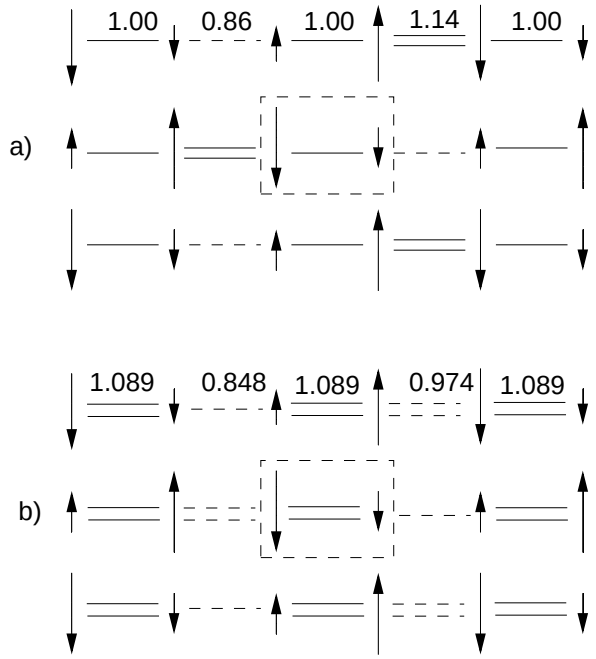

FIG. 2. Sketches of the BCSDW ground states that occur for small $t_\perp$ in the strongly correlated, anisotropic 2D 1/4-filled band. The arrows indicate the spin directions and their sizes indicate the relative charge and spin densities. The hopping integrals used to calculate the energies of the distorted lattices correspond to (a) $r_{4k_F} = 0$ (see text, Section V) and (b) $r_{4k_F} = r_{2k_F}$, and are shown above the bonds along the top chain. This variation in t reflects the BOW. The bond-distortion pattern in (b), with slightly modified weak bond hopping integrals, also corresponds to the dimerized dimer lattice for small enough $t_\perp$. Note that the charge ordering corresponds to the 1D paired electron crystal along the longitudinal *and* both diagonal directions and the the monatomic Wigner crystal along the transverse direction.

explicit numerical calculations to determine that the lowest energy state is obtained with a phase shift of π. The intrachain bond orders, determined by the probabilities of nearest neighbor charge-transfers, continue to be different for the different pairs of neighboring sites. This is the major difference between the possible broken symmetries in the 1/2-filled and 1/4-filled band. While in the 1/2-filled band there is no overlap between the extreme configurations favoring the BOW, CDW and SDW, in the weakly 2D 1/4-filled band *the same extreme configuration supports all three broken symmetries*[24]. For small nonzero $t_\perp$, we therefore expect a strong cooperative coexistence between the BOW, the CDW and the SDW. Furthermore, since the same CDW coexists with both the SUWU BOW and the W′SWS BOW, this coexistence is independent of which particular BOW dominates. This has been explicitly demonstrated in reference [24], where it was shown that the overall ground state for small $t_\perp$ is one of the two BCSDW states shown in Fig. 2, with overall 2D periodicity of ($2k_F$, π).

D. 1/4-filled band, $t_\perp \leq t$, $U, V \neq 0$.

What happens as $t_\perp$ is further increased? Within k-space single-particle theory, increasing $t_\perp$ should destroy the nesting of the Fermi surface. But as we have indicated above, our real space analysis predicts, and our numerical results will establish, that this destruction does not occur. To argue this convincingly, we must first show how this destruction of the nesting, which certainly does occur for non-interacting electrons, can be correctly described within our configuration space picture of the broken symmetry. Recall that the one-electron hopping term in Eq. (1) introduces "paths" between the extreme configurations, where each step in a given path connects two configurations related by a single hop[3,8,20]. Nonzero $t_\perp$ introduces many additional paths connecting the extreme configurations that are the 2D equivalents of ...1100... (with a π-phase shift between consecutive chains). For $U = V = 0$, there is no inhibition of these paths, and it therefore becomes easier to reach one extreme configuration from another, leading to enhanced configuration mixing (relative to 1D), which in its turn destroys the "nesting" and the broken symmetry.

The situation described above changes, however, for nonzero Coulomb interaction. Interchain hopping $t_\perp$ leads to partial double occupancy on a single site ($\uparrow\downarrow$) with an energy barrier that, while less than the bare U, is a U_{eff} that increases with U. The energy barrier to *inter*chain hopping leads to "confinement" of the electrons to single chains, a concept that has been widely debated recently, in the context of high T_c superconductors[33–35]. For large enough U_{eff}, the confinement can be strong enough that the broken symmetry state can persist up to the isotropic limit $t_\perp \sim t$.

More precisely, the bond and charge components of the BCSDW can persist up to the isotropic limit $t_\perp \sim t$, leading to the BCDW state we have previously introduced. The evolution of the spin structure is different from and more subtle than the bond and charge components. From the cartoons in Fig. 2, we see that for the SDW to exist it is essential that the '0's have a spin "direction". In the small $t_\perp$ case, the sign of the spin on a '0' is necessarily that of the nearest *intra*chain '1'. Note, however, that each '0' also has two *inter*chain '1's as neighbors and that for a stable SDW, the spin densities of the '1's that are neighbors of a specific '0' must be opposite (as shown in the Figure). Therefore, with increasing $t_\perp$, competing effects occur. On the one hand, the magnitude of the interchain exchange coupling $J_\perp \sim t_\perp^2/U_{eff}$ increases. On the other hand, the spin density on a site labeled '0' decreases because of the canceling effects of the *intra*- and *inter*-chain neighboring '1's. We thus expect the SDW of the 2D lattice to vanish at a $t_\perp^c$ that will depend on the magnitudes of the bare U and V.

This description of the evolution of the SDW applies to the true 1/4-filled band. In lattices that are dimerized initially, further dimerization leads to the occupancy '10'

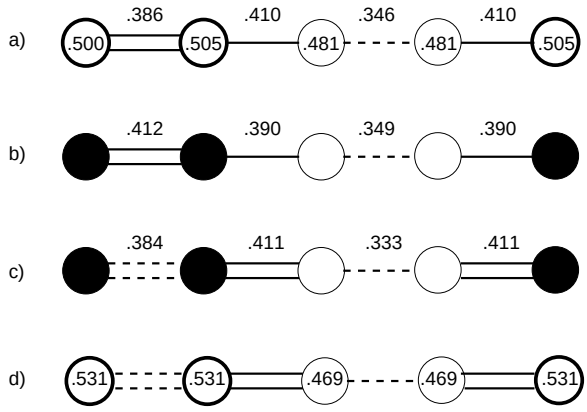

FIG. 3. Numerical results of 1D simulations for $U = 6$, $V = 1$. (a) Charge densities (numbers inside each circle, which represents one molecular site) and bond orders (numbers against the bonds) at the center of an open uniform chain of 16 sites for $\alpha = \beta = 0$. (b) Bond orders in a 16 site periodic ring with uniform hopping, and with externally imposed period 4 magnetic field of the same form as in Fig. 2, with amplitude $\epsilon = 0.05$. (c) Same as in (b) with $\epsilon = 0.1$. Because of equal bond lengths and nonzero V, there is a weak contribution by the ...1010... CDW to the ground state here and the charge densities are not pure ...1100... The filled (unfilled) circles correspond to large (small) charge densities. The bond orders also show weak deviation from pure SUSU or W′SWS behavior, and the bond orders shown are averages for each kind of bond. The magnetic field induced SDW creates a spontaneous BCDW. (d) Charge densities in a periodic dimerized dimer lattice of 16 sites. The double bond corresponds to $t = 1.2$, and the dotted and double dotted bonds to $t = 0.7$ and 0.9, respectively. Note that the CDW pattern in this effective 1/2-filled band system is the same as the 1/4-filled band lattices in (a), (b) and (c).

or '01' on each dimer. If the original dimerization is very strong, the spin on a given '0' will continue to be strongly influenced by the spin on its partner in the dimer, and $t_\perp^c$ at which the SDW vanishes in this case will be larger.

The robustness of the BCSDW and the BCDW relative to the uniform metallic state can be understood from the cartoon occupancy schemes in Fig. 2. It is instructive to discuss the BCDW state in terms of the two large U Wigner crystal structures discussed by Hubbard[50]. We refer to the ...1100... electron arrangement as that of a "paired electron crystal", and the ..1010... as the "monatomic Wigner crystal." For the 3D low density electron gas, Moulopoulos and Ashcroft[57] showed that there exists an intermediate density range where the paired electron crystal has lower energy than the monatomic Wigner crystal, and the region $0 < V < V_c$ in our discrete lattice case can be thought of as intermediate between the $V = 0$ and $V > V_c$. A striking feature of the BCSDW and the BCDW occupancy scheme is that it is a paired electron crystal along the chains (...1100..., periodicity $2k_F$), a monatomic Wigner crystal transverse to the chains (...1010...., periodicity $4k_F$), as well as a paired electron crystal along both diagonals (...1100..., periodicity $2k_F$). It is thus possible to predict that even in the presence of interactions not explicitly included in Eq. (1), the BCDW continues to persist. For instance, by enhancing the $4k_F$ charge ordering along the transverse direction, the nearest neighbor interchain Coulomb interaction $V_\perp$ will further enhance the stability of the BCDW. Similarly, the diagonal ...1100... charge ordering implies that even the additions of hopping t_{diag} and Coulomb repulsion V_{diag} along the diagonals will not destroy the BCDW state for realistic parameters: in particular, V_{diag} stabilizes the BCDW relative to the other Wigner crystal (...1010...) along both x and y directions.

In the above our goal has been to predict a novel semiconducting state that is more stable than the metallic state. Even if this semiconducting state is assumed, however, there is an additional surprise in our claim, viz., the dominance of the singlet BOW over the SDW for strong two-dimensionality in the interacting quarter-filled band. This is *exactly opposite* to what is observed in the 1/2-filled band. While in the half-filled band a single singlet-to-antiferromagnet transition occurs with increasing $t_\perp$, for the 1/4-filled band, a second antiferromagnet-to-singlet transition is predicted at large $t_\perp$. Since a full discussion of this second transition at this junction would interrupt the flow of the narrative, we defer it to Appendix 1, which presents arguments based on variational concepts and valence bond theory to motivate this result.

IV. NUMERICAL RESULTS

A. Results for 1D lattices

Computational limitations will compel us to use fairly small lattices in 2D and will prevent us from studying dynamical phonons (even at a classical, self-consistent level). As a consequence, we will have to work with explicitly distorted lattices, rather than allowing the distortions to arise naturally, as they would in larger lattices calculated with dynamical phonons. To provide justification for this approach, in this section we (a) extend our previous 1D results obtained with nonzero α and β[27] to *zero* e-ph couplings, to demonstrate that these bond and charge distortions are unconditional, and (b) show that the dimerization of the dimer lattice (see Eq. (2)) leads to the same CDW as the monatomic 1/4-filled band.

It is known that in a sufficiently long open chain the bond orders and the charge densities at the center of the chain show the behavior in the long chain limit, even in the absence of the e-ph coupling. In Fig. 3(a) we show the exact nearest neighbor bond orders and charge densities at the center of an open *undistorted* chain of 16 atoms with all hopping integrals equal, for $U = 6$, $V = 1$. Note that both the BOW and the CDW show the $2k_F$ modulations discussed in section III, and appear in spite of uniform hopping integrals.

Second, we recall that in a purely 1D system, a LRO SDW can occur only if an external staggered magnetic field is applied. We therefore incorporate an additional (external field-like) term

$$H_{SDW} = -\sum_j \epsilon[n_{j,\uparrow} cos(2k_F j) + n_{j,\downarrow} cos(2k_F j + \pi/2)] \tag{9}$$

and consider $H + H_{SDW}$ for the 1/4-filled band with amplitude $\epsilon = 0.1$. In reference [27] the same Hamiltonian was investigated for the case of finite bond distortion. Figs. 3(b) and (c) show the bond orders and CDW for a periodic ring (zero e-ph coupling and *undistorted* hopping integrals) with the SDW $\uparrow\downarrow_{\downarrow\uparrow}$ superimposed on it. Note that because of the periodicity, the bond orders are uniform for the finite ring for $\epsilon = 0$. For $\epsilon = 0.05$ (Fig. 3(b)) and 0.1 (Fig. 3(c)), the externally imposed SDW creates *spontaneous* BOWs with $r_{4k_F} = 0$ and $r_{4k_F} \neq 0$, respectively.

In Fig. 3(d) we show the charge densities on a *periodic* ring of 16 sites, now for the dimerized dimer lattice (the hopping integrals here are 1.2, 0.9, 1.2 and 0.7). The charge modulations (which appear entirely due to modulations of the *interdimer* bond orders) on the sites are exactly as in Figs. 3(a)–(c), with the larger charges occurring on the sites connected by the stronger weak bond (the W′ bond, with $t_{W'} = 0.9$). In discussions of the spin-Peierls transition within the effective 1/2-filled band (corresponding to the dimer lattice), it is usually assumed that the electronic populations within each dimer cell remains uniform in the spin-Peierls state. Fig. 3(d) clearly shows that this is not true.

B. Results for 2D lattices

To confirm the expectations based on the qualitative arguments of Section III, we use exact diagonalization and Constrained Path quantum Monte Carlo (CPMC)[58] numerical techniques to calculate for representative finite 2D lattices: (i) the electronic energy gained upon bond distortion,

$$\Delta E \equiv E(0) - E(u_{j,M}), \tag{10}$$

where $E(u_{j,M})$ is the electronic energy per site with *fixed* distortion $u_{j,M}$ along the chains; (ii) the site charge densities $\rho_{j,M}$ for the bond-distorted lattices; due to the coexistence of the BOW and the CDW, measuring the CDW amplitude that results as a consequence of the external modulation of the hopping integrals is exactly equivalent to the measurement of the bond order differences in the charge-modulated lattices; and (iii) the z-z component of the spin-spin correlations, for a range of U, V and $t_\perp$. We consider three distinct distorted lattices, two of which correspond to those shown in Figs. 2(a) and (b), where we have indicated the hopping integrals along the chain (the uniform lattice has a hopping integral of 1.0 corresponding to all intrachain bonds). The third distorted lattice we consider is the dimerized dimer lattice, the hopping integrals for which will be discussed later.

Ideally, calculations that aim to demonstrate persistence of a spatial broken symmetry should do fully self-consistent calculations of the total energy, which is a sum of the the electronic energy gain ΔE (including effects of both e-e and e-ph interactions) and the loss in lattice distortion energy. Unfortunately, in true many-body simulations (such as exact diagonalizations or CPMC) of the very large 2D lattices we investigate (see below), such self-consistent calculations are not possible. A well-tested alternate approach[1] is to calculate only the electronic energy gain for *fixed* lattice distortion and compare the calculated ΔE against a known reference configuration, where the distortion is *known* to occur. This approach works because for a fixed distortion, the contribution of the elastic energy to the total energy is constant, independent of the other parameters; therefore the gain in electronic energy, relative to that for the reference configuration, is a direct measure of the tendency to distortion. An example of a previous successful application of this approach is the enhancement by e-e interactions of the bond alternation in the 1D 1/2-filled band; here, the reference configuration corresponds to the limit of zero e-e interaction (SSH model), where the Peierls bond alternation is known to occur[2]. For nonzero e-e interaction, the electronic energy gain for fixed bond alternation can be larger (see Figs. 2.26 and 2.31 in reference 1), indicating the enhancement of the bond alternation by e-e interaction, a theoretical result that has been confirmed by all subsequent studies. Similarly, in the 2D 1/2-filled band, calculations of the electronic energy gain for fixed bond distortion have been used to prove the *decrease* in the tendency to Peierls bond alternation upon the inclusion of e-e interaction (see Fig. 10 in reference 10), a result that is in agreement with other studies[8,9] as well as the determination of long range AFM in this case[7]. Thus the approach has been shown to work in two cases in which exactly opposite outcomes, – in one case, an increase in dimerization, in the other case, a decrease, occurred, indicating its robustness.

At first glance, it appears that there exist two different reference configurations in the present case. First, for given $t_\perp$, one could study ΔE as a function of U and V: in essence, this amounts to comparing *uncorrelated* and *correlated* lattices for each $t_\perp$. Second, for given U and V, one could calculate ΔE as a function of $t_\perp$. In fact, the first approach does *not* yield correct results for two reasons: (i) the uncorrelated 2D lattices are undistorted, so there is no obvious ΔE with which to compare the correlated results; and (ii) magnitude of ΔE *decreases* with U and V even in the 1D limit, where we *know* that the bond and charge distortions are unconditional (see references 16–19,27, as well as the immediately previous subsection on 1D numerical results). Thus to determine properly the tendency to distortion in 2D, our reference

configuration should be the single chain. We therefore normalize the energy gained for coupled chains (ΔE) against that for the single chain (ΔE_0) with the same U and V. A decreasing $\Delta E/\Delta E_0$ as a function of $t_\perp$ signals the destruction of the distortion by increasing two-dimensionality, while a constant or increasing $\Delta E/\Delta E_0$ indicates a persistent distortion[1,3]. Since the BOW and the CDW are coupled cooperatively, the behavior of the charge ordering gives a second measure for the tendency to bond distortion. Decreasing charge ordering for *fixed* bond distortion, as a function of $t_\perp$ (as occurs for noninteracting electrons), indicates the tendency to decreasing bond distortion, while constant or increasing charge ordering indicates persistent bond distortion. The expected (and calculated, see below) charge ordering pattern is the same for all bond distortion patterns and is the same as in 1D (with, however, a π-phase shift between consecutive chains).

As mentioned above, our numerical calculations involve both exact diagonalization and the CPMC technique. Because of the sign errors that plague quantum Monte Carlo calculations in 2D, it is critical to obtain a precise idea about the accuracy of the numerical results. This is especially so because CPMC calculations that have been reported so far[58,59] are only for the simple Hubbard Hamiltonian and did not include the nearest neighbor interaction V. In Appendix 2 we discuss our methodology and give detailed comparisons of energies and correlation functions obtained for finite lattices within the CPMC and exact diagonalization procedures. As shown there, although the CPMC technique is not variational, the accuracies in both energy and correlation functions are sufficient for our purposes.

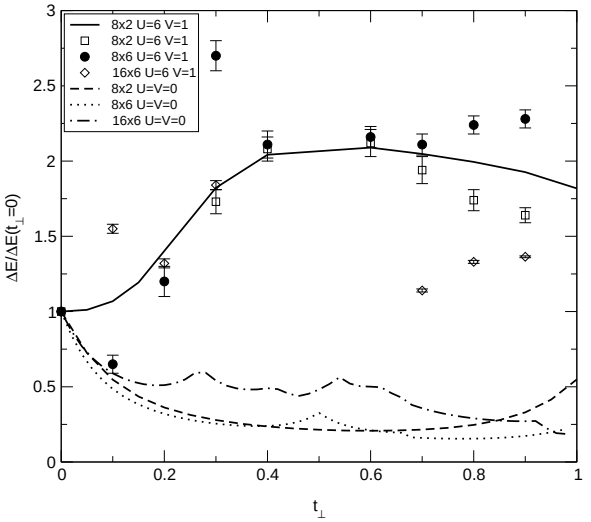

FIG. 4. $\Delta E/\Delta E_0$ versus $t_\perp$ for a $2k_F$ bond distortion ($r_{4k_F} = 0$) for the 8×2, 8×6, and 16×6 lattices for $U = V = 0$ and for $U = 6$, $V = 1$. For the 8×2 lattice both exact (solid line) and CPMC results are shown. Intrachain hopping integrals for the distorted lattices are as indicated in Fig. 2(a).

For numerical results obtained from finite-size calculations to be relevant in the thermodynamic limit, it is essential to choose proper boundary conditions. In the present case, we choose lattices and boundary conditions based on the physical requirement that *for noninteracting electrons any nonzero $t_\perp$ must destabilize the BCDW on that particular finite lattice*. Details of the analysis that guided our choice of 2D lattices are also presented in Appendix 2. There we show N × M lattices

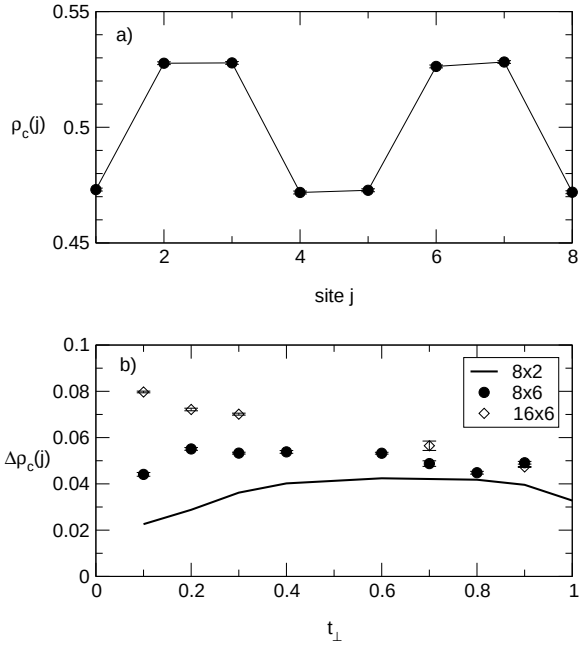

FIG. 5. (a): Site charge densities on one of the 6 chains in a $2k_F$ bond-distorted 8×6 lattice, for $t_\perp = 0.2$, $U = 6$, and $V = 1$. The line is meant as a guide to the eye. Note the expected "..1100.." structure discussed in the text. (b) Amplitude of the $2k_F$ CDW for the $2k_F$ bond-distorted 8×2 (exact), 8×6, and 16×6 lattices. The ground state of the 16×6 lattice is in the S = 1 subspace for $t_\perp > 0.6$, and the CDW amplitudes for the S = 0 states here are expected to be greater than those calculated for the ground state and shown in the Fig. (see text).

(with N the number of sites per chain and M the number of chains) that obey the above physical requirement are restricted to those for which N = 8n, where n is an integer. On the other hand, there is no restriction on M, except that M be even to avoid even/odd effects. In our calculations below, we have chosen M = 4n + 2, for reasons that are also discussed in Appendix 2.

We make one final point before presenting the 2D numerical data. The restriction to N = 8n sites coupled with the 1/4-filling introduces a potential subtlety into the numerical computations of $\Delta E/\Delta E_0$ for nonzero U and V. Finite 4n-electron non-1/2-filled 1D undistorted periodic rings have their ground state in the total spin S = 1 subspace, and even the distorted system's ground state can be in the S = 1 subspace for the smallest 4n-electron rings. We have confirmed from exact

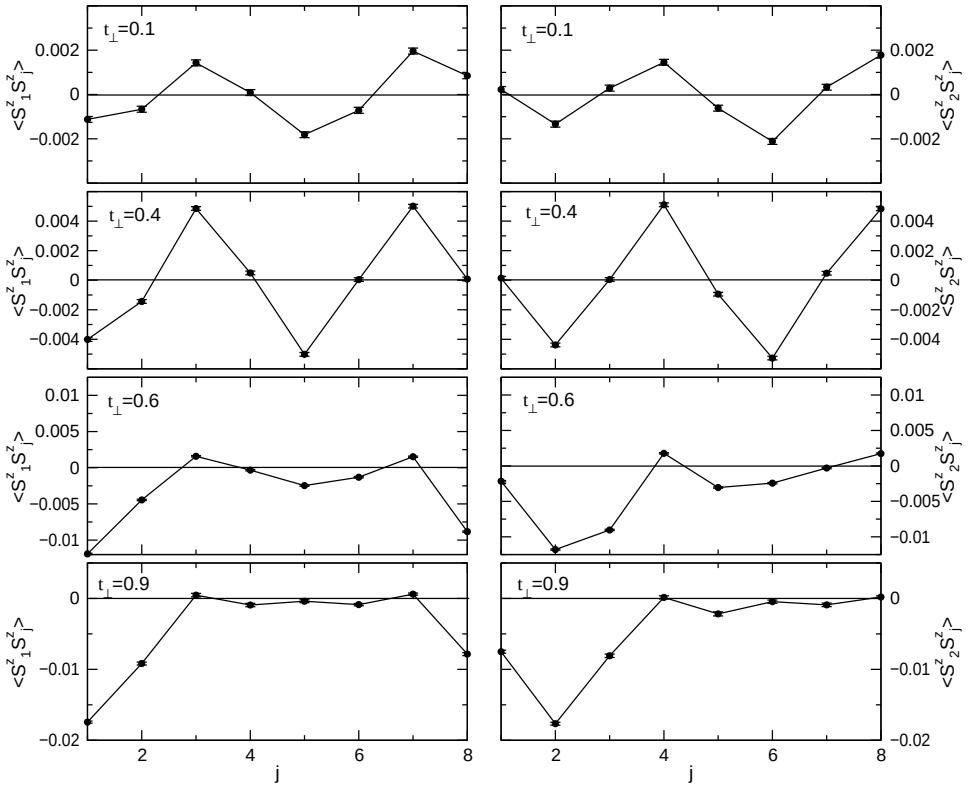

FIG. 6. The z-z spin correlations between sites 1 (left panels) and 2 (right panels) on the first chain of the 8 × 6 lattice and sites j = 1 – 8 on the second chain, with $U = 6$, $V = 1$ for four values of $t_\perp$. Due to finite size effects the wavefunction has small admixing with the ...1010... charge order which affects the individual magnitudes of the spin-spin correlations (see text). AFM correlations increase with $t_\perp$ up to $t_\perp = 0.4$ but then vanish at $t_\perp \simeq 0.6$, even though the BCDW continues to persist for all $t_\perp$ (see Fig. 5). Lines are guides to the eye.

diagonalizations of the 8 × 2 lattice that the ground state is in the S = 0 state for the smallest nonzero $t_\perp$. Thus while ΔE_0 can correspond to the energy gained upon distortion in the S = 1 subspace, ΔE necessarily corresponds to the energy gained upon distortion in the S = 0 subspace. As this important but subtle point requires extensive discussion that would interrupt the presentation here, we present the details in Appendix 3, where we show that despite this subtlety, the behavior of $\Delta E/\Delta E_0$ nevertheless is a proper measure of the stability of the distorted state for nonzero $t_\perp$.

1. Exact diagonalization and CPMC calculations, $r_{4k_F} = 0$

In Fig. 4 we show the behavior of $\Delta E/\Delta E_0$ for the non-interacting and interacting ($U = 6$, $V = 1$) cases for three different lattices satisfying our boundary condition constraints. In all cases we measure the electronic energy gained upon $2k_F$ SUWU bond distortion (corresponding to nearest neighbor hopping integrals $t_S = 1.14$, $t_U = 1.0$, and $t_W = 0.86$), relative to that of the undistorted state with equal hopping integrals. For the 8×2 lattice the calculations involved both exact diagonalization and the CPMC technique. The 8×2 results, taken together, then provide an estimate of the precision of the CPMC calculation. The exact diagonalization studies also confirm that the system is in the total spin state S = 0 for $t_\perp$ as small as 0.01 (see Appendix 3).

The large scatter in the normalized ΔE at very large and very small $t_\perp$ may be due to the degeneracies in the non-interacting system at $t_\perp \to 0$ and $t_\perp \to 1$. Furthermore, as pointed out in Appendix 2 (subsection A), the absolute values of ΔE are rather small, especially for the pure $2k_F$ ($r_{4k_F} = 0$) distortion. The systematic errors due to the CPMC approximation are therefore large in these two regions. Nevertheless, except for the $\Delta E/\Delta E_0$ value at $t_\perp = 0.1$ for the 8×6 lattice, at all other $t_\perp$ the $\Delta E/\Delta E_0$ values are above 1 for all three lattices, and far above the normalized non-interacting values. As seen in Fig. 4, while for the non-interacting cases the $\Delta E/\Delta E_0$ decreases rapidly with $t_\perp$, for the interacting cases the $\Delta E/\Delta E_0$ either remains unchanged or is enhanced by $t_\perp$. Because of the strong degeneracies in the one-electron occupancy scheme at the Fermi level at $t_\perp = 1$, a single well-defined one-electron wavefunction is missing here. The CPMC calculations therefore could not be done for $t_\perp = 1.0$. It is, however, highly unlikely that the BCDW persists for $t_\perp = 0.9$ but vanishes at $t_\perp = 1$; this expectation is corroborated by the results of the exact diagonalization studies for the 8 × 2 lattice, which were performed for the full range of $t_\perp$, including $t_\perp = 1$ and showed enhanced distortion throughout the whole region. In the following sections we also show $\Delta E/\Delta E_0$ for the

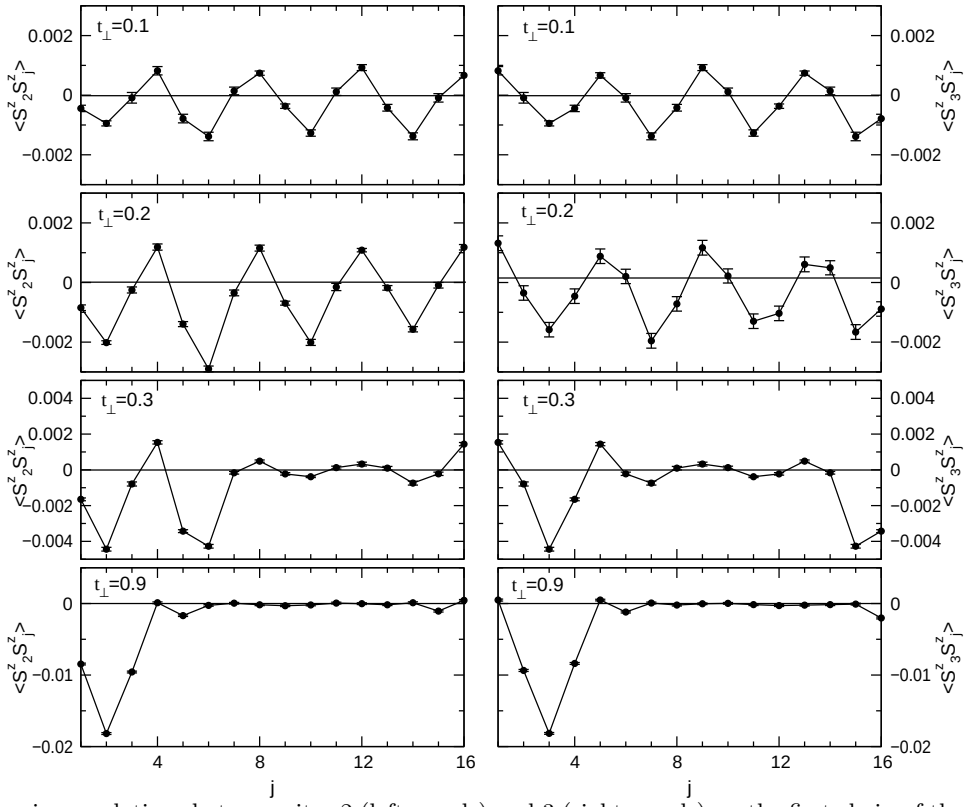

FIG. 7. The z-z spin correlations between sites 2 (left panels) and 3 (right panels) on the first chain of the 16 × 6 lattice and sites j = 1 -16 on the second chain, with $U = 6$, $V = 1$ for four different values of $t_\perp$. The finite size effects, and contamination with the ...1010... charge order here is smaller than in Fig. 6. Lines are guides to the eye.

$2k_F$+$4k_F$ ($r_{4k_F} \neq 0$) and dimerized dimer lattice. In both of these cases, the magnitude of ΔE is larger and hence easier to compute, but degeneracies restrict CPMC simulations to smaller $t_\perp$. In both cases, $\Delta E/\Delta E_0$ is close to or above 1 for all $t_\perp$ we have studied.

As discussed in the above, the bond-distorted lattices (both $r_{4k_F} = 0$ and $r_{4k_F} \neq 0$) have a synergetic coexistence with the CDW. Thus the amplitude of the CDW, defined as $\Delta\rho_c = \rho_{cl} - \rho_{cs}$, where ρ_{cl} and ρ_{cs} are the larger and smaller charge densities on the ...1100... $2k_F$ CDW, is an alternate measure of the stability of the BOW. If the nonzero $t_\perp$ destabilized the bond-distortion, then even with *fixed* $2k_F$ distorted hopping integrals the amplitude of the BOW (measured as the differences in the bond orders) would decrease, and the diminished strength of the BOW in turn would decrease $\Delta\rho_c$. This is easily confirmed for the noninteracting Hamiltonian, where the amplitude of the CDW decreases with increasing $t_\perp$. In Fig. 5(a) we show the charge densities on a single chain for a bond-distorted 8×6 lattice (because of periodicity, all chains are equivalent) for $U = 6$, $V = 1$, and $t_\perp = 0.2$. In Fig. 5(b) we have shown the behavior of $\Delta\rho_c$ for all the three lattices we have studied, now as a function of $t_\perp$. Degeneracies in the one-electron energy levels in the 16×6 lattice for $t_\perp > 0.6$ even with finite bond-distortion cause the CPMC ground states in this region to be S = 1. Exact calculations in the 1D limit show that the amplitude of the CDW in S = 1 is less than that in S = 0. Thus the weak decrease in the $\Delta\rho_c$ values with $t_\perp$ in the 16×6 lattice is a spin effect: the bond distorted state is S = 0 at small $t_\perp$ and S = 1 at large $t_\perp$. The $\Delta\rho_c$ values at large $t_\perp$ for the 16 × 6 lattice should therefore be considered as *lower limits* (the $\Delta\rho_c$ values of the 16 × 6 lattice are considerably larger than that of the S = 1 single chain of 16 sites). In agreement with the behavior of the ΔE in the interacting case (see Fig. 4), the CDW amplitude now *increases* or remains constant with increasing $t_\perp$ for all the lattices studied, indicating a greater tendency to bond and charge distortion with increasing $t_\perp$. *Taken together, the results of Figs. 4 and provide quantitative proof of our qualitative arguments establishing that the BCDW is a robust broken symmetry state for the interacting 2D $\frac{1}{4}$-filled band.*

In Fig. 6 we show the inter-chain spin-spin correlations between sites 1 and 2 on the first chain, and sites j = 1 – 8 on the second chain, for the $2k_F$ bond-distorted 8×6 lattice for several values of $t_\perp$. The SDW profile is somewhat different from what is expected from a pure ...1100... charge modulation along the chains because the wavefunction of this finite lattice also has contributions from the ...1010... type intrachain charge modulation. The small ...1010... contribution to the wavefunction affects the charge density, $n_{j,M,\uparrow} + n_{j,M,\downarrow}$ only weakly, but the spin density, being the difference $n_{j,M,\uparrow} - n_{j,M,\downarrow}$ is a smaller quantity and is affected relatively more strongly. It is useful here to recall however that within the rectangular lattice, ...1010... charge orderings along both longitudinal and transverse directions give triangular lattice

of occupied sites, and thus a pure ...1010... cannot give the SDW profiles of Fig. 6 (see also below)[60].

Qualitatively, at $t_\perp = 0.1$ the SDW behavior is the same as in Ref. 24, where these calculations were done for the 12×4 lattice: the amplitude of the interchain spin-spin correlation is independent of the distance between the sites, indicating long-range order. The qualitative behavior of the spin-spin correlations is the same for $t_\perp = 0.4$, where, however, the amplitude of the SDW is larger. At still larger $t_\perp (= 0.6)$, the inter-chain correlations are very strongly antiferromagnetic at short distances (j = 1,2 on chain 2), but the antiferromagnetic correlations have disappeared at larger distances. This can be seen from comparisons of the spin-spin correlations corresponding to values of j lying near the center of the second chain (j = 5), which are farthest from the spins occupying sites 1 and 2 on the first chain. While the spin-spin correlations near j=5 increase from $t_\perp = 0.1$ to 0.4, they decrease as $t_\perp$ is further increased to 0.6. Similarly, focusing on site 8 of the second chain, we see that the spin-spin correlation with site 1 on the first chain has actually changed sign upon increasing $t_\perp$ to 0.6 from 0.4 (due to the very strong short-range antiferromagnetic correlations), and the magnitude of the positive spin-spin correlation with site 2 on the first chain has decreased. All of these results indicate the absence of long-range spin order for large $t_\perp \geq 0.6$ in the 8×6 lattice. The loss of the long-range spin-order is most clear at $t_\perp = 0.9$, where spin-spin correlations are nonzero only for the nearest interchain neighbors.

Fig. 7 shows the inter-chain spin-spin correlations between sites 2 and 3 on the first chain and sites j=1...16 on the second chain for the 16×6 lattice. The admixture of the intrachain ...1010... CDW is weaker in this larger system: this is because the "tunneling" between the extreme configurations ...1100... and, say, ...0110..., decreases with size, and as consequence, V_c increases with size in finite systems. This can be seen by simply comparing the figures on the left and right panels for $t_\perp = 0.1$ and 0.2. If the intrachain CDW were a pure ...1010...,

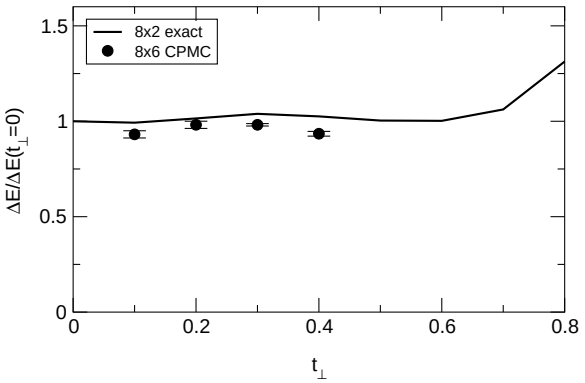

FIG. 8. $\Delta E/\Delta E_0$ versus $t_\perp$ for $r_{4k_F} = r_{2k_F}$ for the 8 × 2 and 8 × 6 lattices for $U = 6$, $V = 1$. Intra-chain hopping integrals for the distorted lattices are as indicated in Fig. 2(b).

the signs of the spin-spin correlations for each j would be the same for both i = 2 and i = 3. Different signs for these correlations are signatures of the ...1100... CDW (see Fig. 2). As in the 8×6 system, long-range SDW behavior is seen for $t_\perp = 0.1$. Focusing on sites j=7 – 12 on the second chain, the amplitude of the SDW increases from $t_\perp = 0.1$ to $t_\perp = 0.2$, but further increasing $t_\perp$ to 0.3 destroys the long-range order, as evidenced again by very large AFM correlations at short distances and vanishing correlations at large distances (sites j=7...12 on the second chain). The vanishing of the SDW is seen most clearly at very large $t_\perp$ ($t_\perp = 0.9$ in Fig. 7). We observe this same behavior of the SDW on 8 × 2 lattice. In all cases, the SDW amplitude initially increases, exhibits a maximum, and then vanishes at a $t_\perp^c$ which decreases with the size of the system. As discussed in section III.D, this behavior is to be expected from the nature of the BCSDW in Fig. 2. The initial increase of the SDW amplitude indicates that $t_\perp^c$ is nonzero, a conclusion that is also in agreement with the experimental observation of the BCSDW state in the weakly 2D organic CTS (see below). Based on the calculations for 16 × 6 lattice, we estimate $0.1 < t_\perp^c < 0.3$ for the strictly rectangular lattice for $U = 6$, $V = 1$.

2. Persistent distortions with $r_{4k_F} \neq 0$

The bond modulation pattern in the 1/4-filled band given in Eq. (7) has in general both $2k_F$ and $4k_F$ components. Figs. 4 and 5 show persistent distortion at large inter-chain couplings for $r_{4k_F} = 0$ (purely $2k_F$ bond distortion). The persistent BCDW is expected also for $r_{4k_F} \neq 0$.

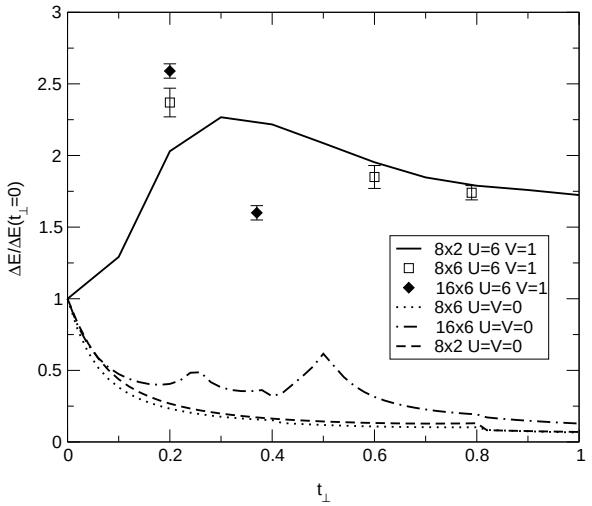

FIG. 9. $\Delta E/\Delta E_0$ versus $t_\perp$ for a dimerized dimer lattice for the 8×2, 8×6 and 16×6 lattices, for $U = 6$, $V = 1$. The intradimer hopping integrals are 1.2 in both cases. All interdimer hopping integrals are 0.8 in the dimer lattice, and 0.7 and 0.9 in the dimerized dimer lattice.

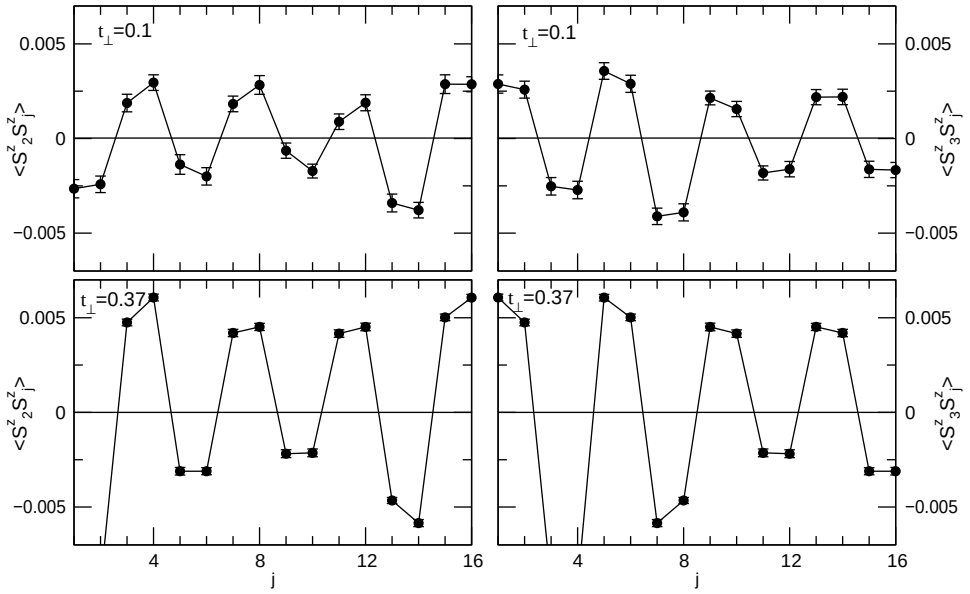

FIG. 10. The z-z spin correlations for the 16×6 dimerized dimer lattice. Correlations are shown between site 2 and site 3 on the first chain and sites 1-16 on the second chain with $U = 6$, $V = 1$ for two values of $t_\perp$ (0.1 and 0.37). Lines are guides to the eye.

Physically, the reason for this persistence is the *coexisting* site CDW, whose nature is independent of r_{4k_F}[24,27]. We show in Fig. 8 the calculated $\Delta E/\Delta E_0$ for $r_{4k_F} = r_{2k_F}$ (equal admixtures of $2k_F$ and $4k_F$ bond distortions), for the 8×2 and 8×6 lattices for $U = 6$ and $V = 1$. The hopping integrals corresponding to the distorted lattice here are 1.089, 0.974, 1.089 and 0.848, and the energy gained is being measured against the uniform lattice. Starting from $t_\perp = 0.5$, the one-electron ΔE is highly discontinuous. This is because distortions with $r_{4k_F} \neq 0$ do not correspond to a natural periodicity for the noninteracting system. As a consequence the noninteracting wavefunctions are not suitable trial wavefunctions for the CPMC calculation. For the same reason the 16×6 calculation could not be performed here. The similarities between the results for the 8×2 and the 8×6 lattices are obvious. The ratio $\Delta E/\Delta E_0$ is independent of $t_\perp$ over a broad range of $t_\perp$ and increases slightly for large $t_\perp$, indicating once again a stable 2D BCDW. Although only limited data could be obtained for this case, the dimerized dimer lattice is very similar in character to $r_{4k_F} \neq 0$ (see Fig. 2(b)). In the following we show convincing evidence for persistent double-dimerization in 2D.

3. The dimerized dimer lattice

We have previously noted that Fig. 2(b) suggests that an alternate way to view the BCDW/BCSDW states is as a dimer lattice with additional structure within each of the dimer cells; the dotted box in Fig. 2(b) represents one dimer. Each dimer has one electron, leading to an "effective half-filled" dimer band[37–40,42]. Bond dimerization in the 1D 1/2-filled band is unconditional for all $U > 2V$[1,3], and thus this dimer lattice itself distorts in a period 2 dimerization pattern in 1D. In this section we show the additional result that the (anisotropic) 2D dimer lattice is unconditionally unstable to a second dimerization for all $t_\perp$.

We choose the hopping integrals between the two sites within the dimer cell to be 1.2 in our calculations. The two inter-dimer hopping integrals for the uniform dimer lattice were taken to be 0.8, while for the distorted ("dimerized") dimer lattice these were taken to be 0.7 and 0.9, respectively (*i.e.*, the dimerized dimer lattice has hopping integrals 1.2, 0.7, 1.2, 0.9 along each chain). Exact diagonalizations show that a π-phase shift between the chains (*i.e.*, dimer cells lying directly above each other, but a strong inter-dimer bond on one chain facing a weak inter-dimer bond on the next chain) gives the lowest total energy. Again we define ΔE and ΔE_0 as the electronic energies gained per site upon interdimer bond distortion by the 2D and 1D lattices. Fig. 9 shows the $\Delta E/\Delta E_0$ behavior for the 8×2 lattice over the complete range of $t_\perp$ and for the 8×6 and 16×6 lattices for several different $t_\perp$ for $U = 6$ and $V = 1$. The 8×6 and 16×6 lattices, taken together, cover nearly the full range of $t_\perp$, and the $\Delta E/\Delta E_0$ behavior for these lattices closely follow the curve for the 8×2 lattice. As before, $\Delta E/\Delta E_0$ is significantly greater than 1 for the complete range $0 < t_\perp < 1$, indicating the persistence of the dimerization of the dimer lattice in the interacting case, whereas for the non-interacting case, the dimerization vanishes, as expected.

Fig. 10 shows the interchain spin-spin correlations between sites 2 and 3 on one chain and sites j = 1 – 16 on a neighboring chain, for a 16×6 dimerized dimer system. Notice the far smaller contribution by the ...1010... intrachain charge ordering here. This is because of the large difference between the hopping integrals even in the "uniform" lattice with interdimer hopping integrals of 0.8 here. Such a large bond dimerization diminishes

the intrachain ...1010... contribution. The spin-spin correlation amplitudes cannot be directly compared to Fig. 7 because of the different distortion amplitudes, but Fig. 10 shows that the SDW amplitude is significantly greater in the intermediate $t_\perp$ regime ($t_\perp = 0.37$ in the Figure) compared to the small $t_\perp$ regime unlike the results in Fig. 7. Our calculations indicate that the larger the difference between the intra-dimer and the inter-dimer hopping integrals, the greater the range of the $t_\perp$ over which the SDW is stable. Thus with hopping integrals of 1.2, 0.9, 1.2 and 0.7 along each chain, the SDW in the 8×6 lattice persists even at $t_\perp = 0.6$ (in contrast to the $2k_F$ bond-distorted lattice of Fig. 2), but vanishes at still larger $t_\perp$. This is expected from our discussion of the behavior of the SDW in Section III.D. Recall that the smaller spin densities on the sites labeled '0' are influenced by both the intrachain nearest neighbor as well as the interchain nearest neighbor with opposite spin, and this competition creates a disordering effect. The larger the hopping integral between the '0' and the nearest intrachain '1', the larger the $t_\perp$ necessary to create the disordering of the spin, hence the greater stability of the SDW. We shall later argue that this same phenomenon is related to the very large magnetic moments of the κ-(BEDT-TTF) salts.

4. Effects of additional Coulomb interactions

Fig. 2 clearly suggests that interchain nearest neighbor Coulomb interaction $V_\perp$ stabilizes the BCDW further. We have confirmed this by exact numerical calculations for the 8 × 2 lattice, as shown in Fig. 11 below, where we have plotted $\Delta E/\Delta E_0$ for three different values of $V_\perp$: 0, 0.5 and 1. Nonzero $V_\perp$ increases ΔE further. Similar calculations were done also with variable $V_\perp$ but fixed $V_\perp/t_\perp$. An even larger increase in ΔE is found in this case. Implementing $V_\perp$ over and above V is difficult within the CPMC, and therefore these calculations could not be performed for larger lattices. However, based on

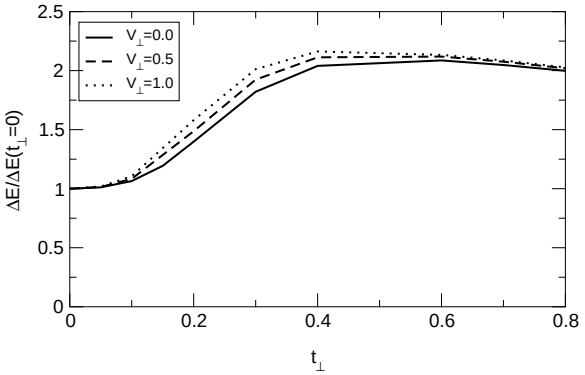

FIG. 11. $\Delta E/\Delta E_0$ vs. $t_\perp$ for the 8 × 2 lattice, with $U = 6$, $V = 1$ and $V_\perp = 0, 0.5, 1.0$, for $r_{4k_F} = 0$.

the similarities between the ΔE behavior of the three lattices studied in Figs. 4 and 9, no difference in the larger lattices is expected.

V. SUMMARY OF THEORETICAL RESULTS

We have performed detailed numerical calculations of various broken symmetries for the 2D 1/4-filled band within Eq. (1) and for the effective 1/2-filled band of dimer lattice within Eq. (2), for $U = 6$, $V = 1$. Regarding these parameter values, the broken symmetries we have found will occur for all intermediate to strong U but require V to be less than a critical $V_c \geq 2t$[51].

We have discovered three distinct new results in 1D. First, we have confirmed that the BCDW state occurs spontaneously even for zero e-ph couplings (see Fig. 3(a)). The bond distortion pattern in the center of a long open chain corresponds to a pure $2k_F$ distortion, and coexists with the $2k_F$ ...1100... type charge modulation. Second, we have shown that a BOW appears spontaneously in a uniform periodic ring when the SDW $\uparrow,\downarrow,_{\downarrow,\uparrow}$ is superimposed, confirming the synergetic cooperation between e-e and e-ph interactions. The BOW pattern corresponds to $r_{4k_F} = 0$ (see Eq. (7)) when the amplitude of the superimposed SDW is relatively weak (Fig. 3(b)), but switches over to $r_{4k_F} \neq 0$ when the SDW amplitude is large (Fig. 3(c)). Our earlier demonstrations of the BOW-SDW coexistence were only for the bond distorted periodic systems. Finally, from exact calculations for a periodic dimerized dimer ring, we have established the new result that the BOW here also coexists with the ...1100... $2k_F$ CDW, with the large (small) charges occupying the sites connected by the stronger (weaker) interdimer W′ (W) bond (see Fig. 3(d)). Our earlier work had claimed that a 1/4-filled description was essential to obtain the BCDW and the BCSDW states. As shown in Fig. 3(d), the same result is obtained, however, even for the dimer lattice, *provided* the second dimerization is allowed to occur.

Three different bond distortion patterns were investigated in 2D. These correspond to $r_{4k_F} = 0$ (Fig. 2(a)), $r_{4k_F} = r_{2k_F}$ (Fig. 2(b)), and the dimerized dimer lattice. In all cases a π-phase shift in the bond distortion between consecutive chains gives the lowest energy. From calculations of energy gained upon bond distortion, we conclude that 2D bond distorted lattices with $r_{4k_F} = 0$ and $r_{4k_F} = r_{2k_F}$ are both more stable than the uniform lattice (see numerical results in Figs. 4 and 8). Similarly, the dimerization of the dimer lattice is also unconditional (see numerical results in Fig. 9). The persistence of the distortions is a novel effect of e-e interactions and is in contradiction to what is expected within one-electron nesting concepts. The ground state of the strongly correlated 1/4-filled band is therefore a novel insulating BCDW state for all $t_\perp$.

The persistence of the BCDW for all anisotropies is also evident from the charge density calculations. In

Fig. 5, we have shown the amplitude of the CDW that accompanies the $r_{4k_F} = 0$ BOW as a function of $t_\perp$. In the absence of e-e interaction, the CDW amplitude decreases rapidly with $t_\perp$ even with nonuniform hopping integrals. One interesting aspect of these calculations is that the CDW pattern is the same for all bond distortion patterns. Our computer capabilities do not allow us to determine self-consistently which of the three BOW patterns dominate within Eqs.(1) and (2) for a given U, V, $t_\perp$, α and β. This is, however, largely irrelevant, because the charge ordering is the same with all the bond distortion patterns.

The SDW behavior is different from those of the BOW and the CDW. As seen from our numerical calculations of interchain spin-spin correlations in Figs. 6 and 7, the SDW amplitude of the novel BCSDW state is initially enhanced by $t_\perp$, but with further increase in $t_\perp$ the SDW vanishes, indicating a singlet BCDW state again in the large $t_\perp$ region. The range of $t_\perp$ within which a stable SDW is found depends on the BOW pattern, and within the dimerized dimer lattice (see Fig. 10) the SDW can be stable over a wider range of $t_\perp$.

VI. COMPARISON TO EXPERIMENTS ON THE INSULATING STATES IN 2:1 ORGANIC CTS

Experimentally, the organic cationic CTS, with cation:anion ratio of 2:1, span the range $t_\perp \leq 0.1$ in $(TMTTF)_2X$ to $t_\perp \sim 1$ in certain $(BEDT\text{-}TTF)_2X$. Hence these materials provide a critical testing ground for our theoretical results. In reference [24], we compared our theoretical predictions regarding the BCSDW state to the mixed CDW-SDW found experimentally in $(TMTTF)_2Br$, $(TMTSF)_2PF_6$ and α-$(BEDT\text{-}TTF)_2KHg(SCN)_4$. Here we make additional, more detailed comparisons, distinguishing between 1D TMTTF and weakly 2D TMTSF-based compounds, and also emphasizing the similarities and differences between the salts of BEDT-TTF and BETS with different crystal structures. In the case of the TMTTF and TMTSF band structure calculations of hopping integrals have been been summarized by Yamaji[61]. In both cases the lattice is anisotropic triangular in nature, which would correspond to our rectangular lattice with one additional diagonal hop t_{diag} beyond the usual $t_\perp$. Both $t_\perp$ and t_{diag} are small in the 1D TMTTF, while they are comparable in TMTSF and about $0.1|t|$ in magnitude. As discussed in section III.D, the paired electron crystal ordering even along the diagonal directions in the configurations shown in Figs. 2(a) and (b) indicate that the BCDW and the BCSDW states continue to be stable for nonzero t_{diag} and there is thus no loss of generality in considering a rectangular lattice. Several crystal structures occur in the BEDT-TTF systems, and more subtle and individual analyses for the different cases are required. Our aim is to show that a variety of recent experiments indicate that the BCSDW and the BCDW are appropriate descriptions of the insulating states of this entire class of 2:1 cationic CTS, and conversely, the very nature of the insulating ground state in certain cases provides direct verification for some of our more surprising theoretical results. We discuss below each class of material individually.

A. $(TMTTF)_2X$

The $(TMTTF)_2X$ compounds are nearly 1D semiconducting materials with weak to moderate dimerization along the stacks at high temperature. Because of this dimerization, they have often been described within the effective 1/2-filled band picture[37,62]. Further dimerization of the dimerization occurs below the SP transition temperature T_{SP} ($\sim$ 15 K). Existing theories of the SP transition in these systems[62] do not discuss the simultaneous appearance of the $2k_F$ CDW and *assume* that the site populations continue to be uniform below T_{SP}. As depicted in Fig. 1(c), and as confirmed in Fig. 3(d), independent of whether these systems are considered as 1/4-filled or effective 1/2-filled with a dimer lattice, the appearance of this $2k_F$ CDW is unconditional and the site populations are therefore not uniform. In a recent NMR study of ^{13}C spin-labeled $(TMTTF)_2PF_6$ and $(TMTTF)_2AsF_6$ charge-ordered states have been found[63]. Although such a charge-ordering suggests agreement with the theory presented here, one problem is that the initial appearance of the charge-ordered phase (at $\sim$ 70 K in $(TMTTF)_2PF_6$) occurs considerably above T_{SP} (15 K)[63]. There are two possible reasons why the charge-ordering might appear at a temperature $T_{CO} > T_{SP}$. First, this might be due to fluctuation effects associated with the 1D nature of the crystals. As has been shown by Schulz[64], fluctuation effects associated with the SP transition may be seen at temperatures as high as $4T_{SP}$, in which case signatures of charge ordering would also become visible at these high temperatures. The observation of diffuse X-ray scattering at $2k_F$ in this material already at $\sim$ 60 K[36,44] seems to support this possibility. A second possibility is that the charge-ordering is driven primarily by the Holstein e-ph coupling β in Hamiltonian (1), and the SSH coupling α is small, such that actual lattice displacement and spin singlet formation takes place at lower temperature. Independent of which mechanism dominates to give $T_{CO} > T_{SP}$, it is important to keep in mind that (a) no charge-ordering is expected at all within conventional theories of SP transition, and (b) as discussed extensively in section III, charge ordering of the type ...1010..., as has sometimes been suggested (see below and footnote 51), promotes equal intrachain bonds, and therefore *the SP transition could not occur if the ...1010...charge-ordering had taken place.* Finally as has been pointed out by us previously[27], charge-ordering of the type ...1100... also occurs in the SP phase of the

anionic 1:2 TCNQ solids.

Although most $(TMTTF)_2X$ exhibit the SP transition, the material $(TMTTF)_2Br$ exhibits a transition to a SDW[65,66], like the $(TMTSF)_2X$. Also like the $(TMTSF)_2X$, this material can become superconducting, although at a relatively high pressure of 26 kbar. Within the structural classification scheme described by Jerome[32], this difference is due to the larger $t_\perp$ in $(TMTTF)_2Br$ (relative to the other TMTTF). We therefore discuss this material along with the $(TMTSF)_2X$.

B. $(TMTTF)_2Br$ and $(TMTSF)_2X$

X-ray scattering studies by Ravy and Pouget[36,44] have shown that in both $(TMTTF)_2Br$ and the prototype TMTSF system, $(TMTSF)_2PF_6$, CDW distortions occur below the SDW transition temperature T_{SDW}. Similar conclusions have been reached also by Kagoshima et al.[45]. In $(TMTTF)_2Br$ evidence for a $4k_F$ lattice instability was found[36,44], clearly suggesting that the insulating state here is the BCSDW of Fig. 2(b). In $(TMTSF)_2PF_6$ the authors claim a "purely electronic CDW", which would indicate the dominance of the $2k_F$ CDW over the BOW. Since, however, in both the 1/4-filled band and the effective 1/2-filled band, the $2k_F$ CDW necessarily coexists with a BOW, the experimental work merely indicates that the transition to the BCSDW state is driven mainly by the Holstein e-ph coupling in Eq. (1) rather than the SSH coupling (*i.e.*, α is small), so that the actual modulations of the intermolecular distances are small[67]. This would agree with one of the two possible reasonings given by us for T_{CO} being larger than T_{SP} in $(TMTTF)_2PF_6$ and $(TMTTF)_2AsF_6$, as discussed above.

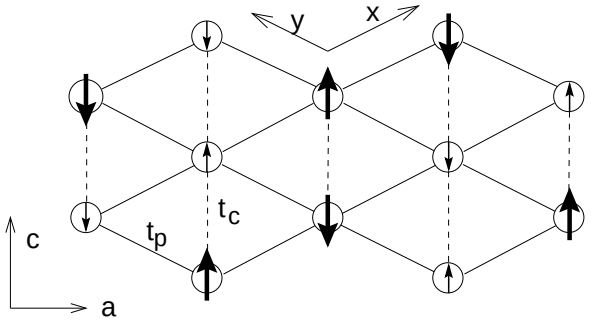

FIG. 12. Schematic view of structure of α-(BEDT-TTF) donor plane from Mori et al.[77] and Ducasse and Fritsch[78]. The solid lines correspond to stronger interstack t_p hopping integrals, the dotted lines to weaker intrastack t_c hopping integrals. The a and c directions indicated are the crystal axes, and the x and y directions correspond to along the chain and perpendicular to the chains in Fig. 2. The arrangement of the spins in the BCSDW state is indicated. Any SDW should be weak because of the nearly isotropic 2D nature of the lattice, but nonvanishing because of the nonzero t_c, which becomes t_{diag} in the x-y coordinate system of Fig. 2 (see text).

One additional comment appears to be necessary. Fröhlich mode sliding conductivity has been seen in $(TMTSF)_2X$[68]. While this indicates a weak incommensurability of the density wave (see below), an equally important point is that the sliding conductivity in the past has been ascribed to a SDW: the SDW collective transport is viewed as that of two CDWs, one for each spin subband. The actual displacement of the charge density is difficult to visualize in configuration space within this picture. We believe that the experimental demonstration of the coexisting CDW and the present theoretical work, taken together, suggest the more coherent viewpoint that the sliding mode conductivity is that of a BCSDW.

C. α-$(BEDT\text{-}TTF)_2MHg(SCN)_4$

This class of materials, with M = K, Rb, Tl and NH_4 has been of considerable interest recently. M = NH_4 is a superconductor, but M = K, Rb, Tl are non-superconducting. Early magnetic susceptibility studies in the M = K material had indicated anisotropic susceptibility below the so-called "kink" transition that occurs at 10 K, indicating a SDW; here the kink refers to the change in slope that occurs in the temperature dependence of the resistivity and the Hall coefficient. On the other hand, analysis of the angle-dependent magnetoresistance oscillations by Sasaki and Toyota led these authors to conclude already in 1995, prior to the experiments by Pouget and Ravy in the $(TMTSF)_2PF_6$, that the dominant broken symmetry in α-$(BEDT\text{-}TTF)_2MHg(SCN)_4$ is a CDW[69]. Since, however, a CDW would not explain the anisotropic susceptibility, Sasaki and Toyota concluded that the broken symmetry here is a "mysterious" state that is a "SDW accompanied by a CDW" or a "CDW accompanied by a SDW". Muon spin resonance studies indicate very small magnetic moment per BEDT-TTF molecule here, ~ 0.003 μ_B[70] (to be compared against 0.08 μ_B in $(TMTSF)_2X$[71] and 0.4 – 1 μ_B per BEDT-TTF dimer in κ-$(BEDT\text{-}TTF)_2Cu(CN)_2Cl$[72], see below). More recent ^{13}C-NMR studies in the M = Rb indicate even smaller magnetic moment (if it exists at all) $\sim 1 \times 10^{-4}$ μ_B[73]. Recent theoretical[74] and experimental[75] investigations conclude either that the dominant broken symmetry here is a CDW or that it is not a conventional SDW[76].

We point out here that a mixed state with very small magnetic moments is exactly what is expected within our theory. In Fig. 12 we have given a schematic view of the structure of the donor plane in α-$(BEDT\text{-}TTF)_2MHg(SCN)_4$. The one-electron hopping integrals (called "t_p" and "t_c" in the figure) have been calculated using approximate one-electron techniques by Mori et al.[77] and Ducasse and Fritsch[78]. Here the t_p correspond to the interstack hopping and the t_c to the intrastack hopping. Four slightly different p-type integrals and three slightly different c-type integrals are obtained

by these authors. We ignore the small differences within each type of hopping integrals, as a more important effect is the periodic modulation that appears with the BCDW. We believe that what is relevant in the present context is that $t_p > t_c$. The α-BEDT-TTF lattice is then simply a rotated (by approximately 45^o) version of our rectangular lattice with both t and $t_\perp = t_p$ and $t_{diag} = t_c$. Our calculations (see Figs. 4, 5, 8 and 9) show that even at $t_\perp \sim 1$ the correlated 1/4-filled band (or the dimerized dimer lattice) remains bond and charge-distorted, while based on the ..1100... ordering along the diagonals we have argued that t_{diag} does not destroy this order (see section III.D). Furthermore, while $t_\perp > t_\perp^c$ destroys the SDW order (leaving the BCDW intact) by disordering the spins on the sites labeled '0' (see section III), a small t_{diag} will have a tendency to restore it, since now each small spin has two neighbors with spins of the same sign and one spin with opposite sign. Thus, the experimentally observed strong BCDW and a weak nearly vanishing SDW is exactly what we expect within our theory. Further evidence for a partial gap has been found in the ^{13}C-NMR studies of α-(BEDT-TTF)$_2$KHg(SCN)$_4$ in high magnetic fields, in a region where the system was previously thought to be a metal[76]. In Fig. 12 we give a schematic of the spin arrangement in the α-BEDT-TTF lattice; note that the underlying $x \leftrightarrow y$ symmetry in the isotropic 2D limit implies that there are two degenerate orthogonal 2D BCDW states here.

Since in α-(BEDT-TTF)$_2$MHg(SCN)$_4$ charge-ordering has also been discussed by Kino and Fukuyama[39], and more recently, by Seo[79], we should point out that the charge-ordering proposed by these authors is different from that in Fig. 12. Our charge-ordering in Fig. 12 is a rotated version of Fig. 2, where the occupancy scheme is ...1100... along the x-direction and along the diagonals. The charge-ordering found by Kino and Fukuyama, and by Seo, assumes that the ...1010... order dominates over the ...1100... order. The ordering determined by Kino and Fukuyama is within a Hartree-Fock solution to the simple Hubbard model (zero intersite Coulomb interaction and zero e-ph coupling) and consists of a stripe structure with stack occupancies (c-direction in Fig. 12) alternating, *i.e.*, stacks are either completely filled or completely devoid of holes). More recently, Seo has repeated these calculations by incorporating nearest neighbor Coulomb interaction V, but by treating U within the Hartree-Fock approximation and the V within the Hartree approximation. Different stripe structures, including that of Fukuyama and Kino, are found now, but once again, these are derived fundamentally from the occupancy scheme ...1010... As has, however, been pointed out by previous authors[19,27], the ...1010... charge ordering for the case of $V = 0$ is an artifact of the Hartree-Fock approximation. Similarly, the Hartree approximation for V also exaggerates the ...1010... order while the Hartree-Fock treatment of the Hubbard term exaggerates the SDW order[51]. This is precisely why these authors find very large magnetic moments in the α-phase materials, in disagreement with experiments.

D. κ-(BEDT-TTF)$_2$X

The deviation from the rectangular lattice is much stronger here[31]. Crystal structure effects are very strong, and as a consequence the lattice is strongly dimerized, with the dimer sites forming an effective triangular lattice[39]. The strong deviation from the rectangular lattice precludes direct comparisons against our theory. A more elaborate discussion of the spin arrangement will be given elsewhere. Here we only point out that (a) our calculations with the dimerized dimer lattice indicate that very large spin moments are possible when the intra-dimer hopping integrals are large compared to the inter-dimer hopping (see Fig. 10), in qualitative agreement with the observed very large magnetic moment in κ-(BEDT-TTF)$_2$Cu(CN)$_2$Cl[72], and (b) each dimer of BEDT-TTF molecules has the cartoon occupancy of 10 or 01 and the ...1100... ordering along one direction and ...1010... ordering along another (see Fig. 2), thereby reducing the spin frustration among the dimer sites forming the triangular lattice. In the absence of this population difference within each dimer cell (and the population difference is a consequence only of dimerization of the dimer lattice) the frustration within the triangular lattice would have severely reduced magnetic moments. We further point out that a pseudo-gap in the spectrum of magnetic excitations has been observed in the SDW phase of κ-(BEDT-TTF)$_2$Cu[N(CN)$_2$]Br[80–82] and κ-(BEDT-TTF)$_2$Cu(NCS)$_2$[81]; this is in agreement with the dimerization of the dimer lattice, since without the second dimerization there should be no spin gap within the 2D antiferromagnet.

The material κ-(BEDT-TTF)$_2$Cu$_2$(CN)$_3$ merits separate discussion. This material is not antiferromagnetic, and measurement of spin susceptibility due to the BEDT-TTF components exhibits a steep drop below 10 K, suggesting SP-like behavior[83]. This behavior is very similar to that in the BETS-based materials, which we discuss below, where we point out that for $\rho = 1/2$, this behavior is expected for the case of large $t_\perp$ ($> t_\perp^c$).

E. λ-(BETS)$_2$GaBr$_z$Cl$_{4-z}$ (BETS = BEDT-TSF)

These materials, discovered only recently[84–86], are superconducting for $0 < z \leq 0.8$ and semiconducting for $0.8 < z < 2.0$. Thus the proximity between a semiconducting and a superconducting state that characterizes the TMTSF and the BEDT-TTF is also a characteristic feature of the λ-BETS. In contrast to the TMTSF and the BEDT-TTF systems, however, the semiconducting state in the BETS is *nonmagnetic* and possesses a spin gap[87]. Magnetic susceptibility studies indicate absence of anisotropy in the susceptibility, and no spin-flop

transition (signature of antiferromagnetism) was found down to 10 K, which is close to the maximum superconducting critical temperature T_c (onset 7.5 K, and even higher in certain samples)[84]. The absence of the SDW is particularly perplexing here in view of the strong two-dimensionality predicted within extended Hückel band calculations[86].

The lattice structures of the λ-$(BETS)_2GaBr_zCl_{4-z}$ are known[84]. The stacking of the organic donor molecules is very similar to the β-BEDT-TTF systems, *i.e.*, a nearly rectangular lattice with strong intrastack coupling, weaker transverse coupling, and very weak coupling along one diagonal. The nearly rectangular lattice permits comparison with our theory. One interesting feature of the lattice structure is that the intrastack bonds have strengths that are W′SWS, exactly the structure expected for the $r_{4k_F} \neq 0$ lattice in Fig. 2(b) as well as the dimerized dimer lattice. We believe that while the difference between the strong and weak bonds is a crystal structure effect, the further dimerization of the dimer lattice is a consequence of the BCDW instability discussed here.

Hartree-Fock calculations by Seo and Fukuyama[88] within an anisotropic Hubbard Hamiltonian gave an antiferromagnetic ground state instead of the nonmagnetic state. Since Hartree-Fock calculations overestimate antiferromagnetism, these authors then chose the $U \to \infty$ limit of Hubbard model to arrive at a dimerized, anisotropic 2D Heisenberg spin Hamiltonian, each lattice site of which corresponds to one dimer of the original BETS lattice. The antiferromagnetic-SP boundary within the 2D dimerized Heisenberg spin Hamiltonian has been investigated by Katoh and Imada using QMC simulations[89]. For the longitudinal and transverse exchange integrals derived by Seo and Fukuyama, the QMC calculations still predict the antiferromagnetic structure[88]. Seo and Fukuyama explain the spin gap in λ-BETS by claiming that the second dimerization of the dimer lattice (*i.e.*, intermolecular distances W′SWS, instead of WSWS) takes these systems to the 1D side of the 1D-2D antiferromagnetic-SP boundary, exactly as $(TMTTF)_2PF_6$, even though the actual transverse hopping integrals are large.

We believe that the problem faced by these authors arises entirely from their effective 1/2-filled band approximation. As seen in Fig. 10, the dimerization of the dimer lattice enhances the SDW in the region of small to intermediate $t_\perp$ and therefore cannot be the origin of the spin gap or supposedly 1D behavior. Recall also that $(TMTTF)_2PF_6$, which is certainly on the 1D side of the 1D-2D boundary, is nonsuperconducting. In contrast, λ-BETS does become superconducting and that too at a T_c that is considerably higher than that in the $(TMTSF)_2X$, indicating what we believe to be strongly 2D character[86]. We believe that the solution to this puzzle lies in recognizing the $\rho = 1/2$ character of the $(BETS)_2X$. An essential difference between the effective 1/2-filled band model of Seo and Fukuyama and ours is that within the former, there are only two regions, nearly 1D and 2D, with the spin states as singlet and antiferromagnetic, respectively. Our work indicates that there are three distinct regions, singlet, antiferromagnet, and singlet again, as a function of increasing $t_\perp$, independent of whether one assumes a 1/4-filled band or an effective 1/2-filled band. We therefore believe that a more natural explanation of the spin gap phase is obtained within our theory, with the singlet ground state in semiconducting BETS not being due to $t_\perp$ that is too small, *but due to a $t_\perp$ that is too large ($> t_c$)* to give SDW. This would be in agreement with the strong two-dimensionality of these systems[84,86]. We believe that the same explanation also applies to the κ-$(BEDT\text{-}TTF)_2Cu_2(CN)_3$, discussed in the above. We predict that experiments that can probe charge ordering will find two kinds of BETS molecules with different electronic populations, with greater charge densities on the two BETS molecules that are linked by the W′ bond.

VII. POSSIBLE IMPLICATIONS FOR ORGANIC SUPERCONDUCTIVITY

What might be the implications of our BCSDW and BCDW states to organic superconductivity, the mechanism for which remains unclear despite two decades of research? We present here several partial responses to this challenging question.

First, given the the robustness of the BCDW/BCSDW in the exactly 1/4-filled band, we believe that the superconductivity must be the result of weak incommensurability in the actual materials. Specifically, we suggest and discuss in more detail below, that superconductivity arises from the pairing of commensurability defects in the background BCDW/BCSDW. That such weak incommensurability exists is strongly indicated by (i) the observation of a zero-energy mode in the optical conductivity[90,91] of $(TMTSF)_2PF_6$ and $(TMTSF)_2ClO_4$; (ii) the observation of Fröhlich mode sliding transport in the same materials[68]; and (iii) the observation of a "partially gapped Fermi surface" in the metallic region[76] of α-$(BEDT\text{-}TTF)_2KHg(SCN)_4$. Extremely interesting results in this context were reported by Komatsu et. al.[83], who showed that the superconductivity in κ-$(BEDT\text{-}TTF)_2Cu_2(CN)_3$ was due to a subtle change in the valence state of the Cu. The pure κ-phase material is a semiconductor with the Cu valence of +1. According to the authors of Ref. 83, the superconducting phase corresponds to a different material (κ' in the authors' notation) in which some of the Cu (several hundred ppm) have acquired valency 2+. This was confirmed from ESR studies. The increase in Cu valency decreases the overall negative charge on the anion, and therefore the overall positive charge on the cation, providing a weak incommensurability that appears to be essential for superconductivity[83]. This result lends credence to our suggestion that organic superconductivity arises

from the pairing of commensurability defects within the BCDW/BCSDW background.

Second, the similarities between the organic and high temperature oxide superconductors have been pointed out in recent years by several research groups[40,92–95]. One obvious apparent similarity between these two classes of superconductors is the proximity of the SDW to superconductivity. Our studies suggest that superconductivity in the organics is actually occurring at the interface of a Coulomb-induced BCDW that for a range of $t_\perp$ coexists with the SDW. It therefore seems more likely that the pair binding is actually driven by the BCDW, and not the SDW, although it is probable that the symmetry of the pairing state may depend on the SDW (see below). As noted above, the experimental observation of superconductivity in the λ-$(BETS)_2GaCl_4$ (where no proximate SDW is observed[87]) supports this view. An important implication of this perspective is that it casts doubt on recent spin-fluctuation theories of *organic* superconductivity within the effective 1/2-filled correlated electron model[96–100]. The consequences of this conclusion from the organics for the high T_c materials are unclear, but it is perhaps not irrelevant in this context to point out that evidence for superconductivity within the 2D nearly 1/2-filled Hubbard model, which for large U has strongly AFM behavior, has remained elusive[101–103], despite more than a decade of intense research[104,105].

Third, there are striking similarities between this "doped" BCSDW/BCDW scenario and several other theoretical suggestions of superconductivity induced by doping of exotic "paired" semiconductors. As we have noted previously, the BCSDW and the BCDW states are very similar to the "paired electron crystal" (as opposed to the monatomic Wigner crystal) found by Moulopoulos and Ashcroft for the intermediate density electron gas[57]. Superconductivity near the "melting" transition of the paired electron crystal has been conjectured by a number of authors in the past[106–109], even before the discovery of organic or high T_c superconductivity. The commensurate BCDW is also qualitatively similar to a "negative U - positive V" effective 1/2-filled extended Hubbard model, with the effective lattice sites sites consisting of (a) the "occupied" pair ('1–1') of nearest neighbor sites, and (b) the "unoccupied" pair ('0–0') of nearest neighbor sites, in Fig. 1(c). Within this scenario, there is an effective attraction between the carriers on the "occupied" pair of dimer sites, but an effective repulsion between two pairs of occupied dimers. For models of this type, it is known that diagonal and off-diagonal long-range order can in principle coexist slightly away from commensurate filling[110–112]. Further, Imada has studied[113] a 2D spin-Peierls state (not possible in the monatomic 1/2-filled band) in which each composite site is again a dimer, with the dimer sites now having occupancies '10' and '01' (see Fig. 2(b) and note that the bonds between a '10' and '01' and between a '01' and a '10' are different, giving rise to a spin-Peierls-like behavior). His numerical simulations find evidence for superconductivity in the hypothetical doped 2D spin-Peierls state[113]. Finally, Emery, Fradkin, and Kivelson have recently suggested[114] that superconductivity can exist for incommensurate fillings in models that support stripe phases and in which a spin gap is present. Since the analysis in Ref. 114 does not make direct contact with an initial microscopic Hamiltonian, but rather posits the form of the effective Hamiltonian in the vicinity of an unpinned stripe phase, it is not possible immediately to make detailed comparisons with our results. We can, however, make two comments. First, Ref. 114 reflects the widespread belief that models within which a spin gap persists in the doped state are strong candidates for a microscopic theory of correlated superconductivity. Our preliminary numerical evidence suggests that both the BCDW and the BCSDW will continue to have a spin gap when doped; further work is in progress to confirm this. Second, regarding the attractive possibility that our BCSDW/BCDW state provides the background charge order within which commensurability defects may pair to form a superconducting state, we note that the occupancy schemes in Fig. 1(c) and Fig. 2(a) and (b) resemble intersecting stripes, where each stripe is obtained by connecting the '1–1' bonds along the x- and x+y (–x+y) directions.

The possible BCSDW/BCDW to superconductor transition in the organic CTS clearly requires further study. We close our present discussion of this topic with comments on three important open issues: (i) the possible mechanism for superconducting pairing; (ii) the problem of phase separation; and (iii) the symmetry of the order parameter.

First, the possible mechanism for pairing of commensurability defects within the 2D BCDW can be visualized most simply in the rigid bond limit, where nearest-neighbor bonds retain their individual distortions independent of the occupancies of the sites linked by these bonds. The commensurate BCDW in this limit can be viewed as consisting of "quasimolecules", where each quasimolecule is a "1-1" dimer. If two holes are now removed from the system, it is energetically preferable to destroy one "quasichemical bond," thereby creating an intersite (small) bipolaron, as opposed to destroying two bonds and creating two polarons. Thus, within the W′SWS structure ($t_S > t_{W'} > t_W$), each W′ bond acts as a "negative-U" center in the rigid bond limit. It is of course highly unlikely that superconductivity can be obtained, at least at the experimental T_c, due to condensation of small bipolarons[111], so this might appear to present a serious problem for this proposed mechanism. In fact, when one goes beyond the oversimplified rigid bond limit to the full model that correctly reflects the cooperation between e-e and e-ph interactions in the 1/4-filled band, one finds that the actual commensurability defects are more like the extended, "resonant" (and therefore mobile) bipolarons that are indeed candidates for explaining superconductivity in strongly correlated systems[111,112]. To understand this in detail, consider again the weakly incommensurate BCDW, starting from

the 1D limit, but now with the e-ph interactions included. Below the $4k_F$ transition temperature T_{4k_F}, but above the $2k_F$ transition temperature T_{2k_F}, incommensurability leads to *fractionally charged* solitons with charge e/2, and each vacancy creates two such defects[115,116]. Previous work has assumed that the soliton charge remains e/2 even below the $2k_F$ transition, which implies that two vacancies create four such defects[116]. However, Ref. 116 assumes that the site charge density remains uniform even below the 1D $2k_F$ SP (dimerization of the dimer lattice) transition, which is precisely what we have shown here not to be the case. Indeed, as a consequence of this spatial charge inhomogeneity (charge ordering), the "solitons" now acquire integer charge (*i.e.*, two fractionally charged solitons bind to give a single soliton with charge +e), as we have shown explicitly elsewhere[117]. A pair of added vacancies within the 1D BCDW below T_{2k_F} therefore creates (only) two solitons. In the strictly 1D limit, these do not bind, but with increasing $t_\perp$, one expects binding to a *large* bipolaron. The source of this binding is precisely the same as the source of soliton confinement in coupled chains of polyacetylene[1]: in the region between the two defect centers the phase relationships between the BCDW's on neighboring chains is different from the preferred one (viz., π), and therefore a large separation between the defect centers would increase the energy (linearly with increasing separation). There exists therefore a *space-dependent* interaction between the polarons, which is repulsive at short range but attractive at some ($t_\perp$-dependent) intermediate range. The bipolaron size, as well as its dimensionality, depends on $t_\perp$ (as well as on U and V). There is currently limited analysis of 2D large bipolarons in the strongly correlated limit, although some results suggest that these can indeed be mobile[112]. Within this scenario, superconductivity occurs due to the condensation of these large bipolarons, which is *not* precluded by the theoretical analysis of Ref. 111. Resolving the question of whether static distortion is sufficient, or whether dynamical phonons will have to be included, will require further work.

Second, in many existing models of superconducting pairing involving correlated electrons, the interactions that bind two particles also lead to phase separation, since the attraction producing pairing does not saturate. Perhaps the best known example of this is the t-J model[104,118] away from 1/2-filling. In contrast, within any "negative U" model there does exist a saturation in this attraction (since a single site can at most have two electrons), and the analogy between our BCDW model and the effective 1/2-filled "negative U – positive V" case suggests that phase separation will also not occur here. Further, the immediately previous discussion of the proposed binding mechanism makes clear that with small but macroscopic (say, 1%) concentration of commensurability defects, there is no particular energetic advantage in creating additional polarons or bipolarons proximate to the original bipolaron (in contrast to, say, the t-J model, where there *is* such an energetic advantage).

Third, what symmetry do we expect for the superconducting order parameter in our model? This is clearly a challenging issue, particularly since even with the *same* BCDW background the pairing symmetry in the highly anisotropic TMTSF *might* be different from that in the more two-dimensional BEDT-TTF and BETS. Several recent experiments have presented evidence consistent with nodes in the superconducting gap function in the BEDT-TTF[119–122]. This is reminiscent of d-wave symmetry of the superconducting order parameter in the high temperature copper oxide based superconductors. On the other hand, Lee at al. have recently presented evidence[123,124] suggesting that a spin triplet p-wave pairing is necessary to explain data in $(TMTSF)_2PF_6$, where the upper critical field H_{c2} shows no saturation with the field in the plane of the organic molecules and exceeds the Pauli paramagnetic (Clogston) limit expected to hold for singlet superconductors[123] and the temperature dependent Knight shift measurements of ^{77}Se show that the spin susceptibility remains unaltered through the superconducting T_c[124]. Within the continuum RG theories[16,17] triplet superconductivity does indeed occur proximate to the SDW. However, within the discrete extended Hubbard model, triplet superconductivity occurs within a very narrow region of the the "positive U – negative V" sector of the $U-V$ phase diagram, bounded by the SDW phase and a phase segregated phase[55]. Triplet pairing thus will not only require a change in sign of the nearest neighbor Coulomb interaction within our original Hamiltonian of Eq. (1), but will also occur for a very narrow critical range of this parameter. But to resolve definitively the issue of the symmetry of the order parameter within our model will be a non-trivial task, as the consequences of the interplay between e-e and e-ph interactions, as well as the effects of anisotropy, must be properly understood.

VIII. ACKNOWLEDGMENTS

We thank Jim Gubernatis and Shiwei Zhang for discussions regarding the CPMC method, Eduardo Fradkin and Philip Phillips for discussions of their recent theoretical results, and Stuart Brown, Paul Chaikin, and Andrew Schwarz for discussions of their experiments. We also acknowledge stimulating discussions with Zlatko Tesanovic. Work at the University of Illinois was supported in part by the grants NSF-DMR-97-12765 and NSF-GER-93-54978 and by an allocation of supercomputer time through the NRAC program of the NCSA.

APPENDIX 1: THE AFM-SINGLET TRANSITION FOR WEAK ANISOTROPY

Our goal here is to understand the second AFM-to-singlet transition that should occur in the quarter-filled

band for large $t_\perp$ from a perspective that is different from the one presented in section III. Specifically, we refer to the antiferromagnetic dimer lattice of Fig. 1(b) with weak intrachain interdimer links, and the frozen valence bond state of Fig. 1(c), in which one of the interdimer links (W′ in the notation of section III) is now stronger than the other (W in the notation of section III), and is a singlet bond. We aim to give variational arguments at the simplest level that (a) point out the difference between $\rho = 1$ and $\rho = 1/2$, and (b) indicate that the frozen valence bond state of Fig. 1(c) dominates over the antiferromagnetic dimer lattice of Fig. 1(b) for large $t_\perp$ and therefore the dimerization of the dimer lattice is unconditional. The argument given below is not to be considered as a proof, but rather, it provides convincing physical motivation for the numerical work discussed in section IV.

Note that our discussion here is limited to the relative stabilities of two insulating states, and not the competition with any metallic state. We consider only the simple Hubbard Hamiltonian with $V = 0$ (since for $\rho = 1/2$ the periodicity of the CDW is the same for all $V < V_c$ and while for $\rho = 1$ the V merely reduces the effective on-site correlation) for $t_\perp = 1$. For completeness we begin by repeating the variational argument for the dominance of the SDW over the BOW in $\rho = 1$. Consider the Heisenberg antiferromagnetic spin Hamiltonian

$$H = J \sum_{\langle ij \rangle} S_i . S_j \tag{11}$$

Consider also the singlet variational state (1,2)(3,4)....(N-1,N), with singlet bonds between nearest neighbors in 1D and the Néel state ... $\uparrow\downarrow\uparrow\downarrow$ .... The energy of an isolated singlet bond is –(3/4)J while that of a 2-site Néel state is –(1/4)J. The overall variational energy of the singlet state in 1D is –(3/8)NJ and that of the Néel state –(1/4)NJ, so that the singlet dominates over the Néel state in 1D. In the 2D isotropic N × N lattice, we compare (1) the frozen valence bond state in which each chain still has the same spin couplings as in 1D (note that at the level of our approximation the relative phases between consecutive chains make no difference), and (2) the 2D Néel state. The variational energy of the frozen valence bond state is –(3/8)N^2J, but now because of the larger number of nearest neighbors the energy of the Néel state has a lower value –(1/2)N^2J, which therefore dominates over the frozen valence bond state. Thus for $\rho = 1$ in 1D the SP state dominates, while in 2D the SDW wins over the SP state. While this argument may appear simplistic, it nevertheless predicts the dominance of the antiferromagnet over the singlet in $\rho = 1$.

Consider now the isotropic 2D *dimerized* $\rho = 1/2$ lattice with moderately strong dimerization (Fig. 1(b)). The effective 1/2-filled band is clearly a SDW, with the dimerization pattern being necessarily "in-phase" between consecutive chains, as shown in Fig. 1(b) (to prevent confusion in what follows we have not shown the bonds in Fig. 1(b), but a strong bond between the two sites within the parentheses and weaker interdimer bonds have been assumed) The individual site populations are equal in this state and each is exactly 1/2. Our contention is that this state has a *higher* variational energy than that reached by further dimerization of the dimer lattice, which gives the $\rho = 1/2$ frozen valence bond state shown in Fig. 1(c), where there occur interdimer singlet bonds and site occupancies ...1100... (the singlet bonds in Fig. 1(c) are between the "occupied" sites). The reason for this is that unlike in $\rho = 1$, the exchange integrals that describe the effective Heisenberg models in the SDW and the singlet are now *different*, in spite of the fact that both Heisenberg systems are derived from the same Hubbard Hamiltonian. In Fig. 1(c), we are considering isolated singlet bonds, with site occupancies of 1, and J is clearly $2t^2/U$, exactly as for $\rho = 1$. In Fig. 1(b), on the other hand, the exchange integral has to correspond to a true $\rho = 1/2$ system, since each site occupancy is now 1/2. The exchange integral J′ for arbitrary ρ in 1D is $2(t^2/U)\rho[1 - sin(2\pi\rho/)2\pi\rho]$[52], so that for $\rho = 1/2$ we have J′ = (1/2)J along each chain (the x-direction). This expression is strictly true only in the 1D undistorted chain, and for the distorted 1D chain or in 2D one needs to calculate J′ from comparing singlet-triplet gaps within the structure corresponding to Fig. 1(b) and within the 1/2-filled band. We have calculated these gaps for finite lattices separately for the longitudinal and transverse directions and have found that while J′ = (1/2)J is quite accurate for the longitudinal direction, the J′ in the transverse direction is *even smaller* (the difference between the longitudinal and transverse directions originates from dimerization along the longitudinal direction only), with the restriction that only interdimer hops lead to spin exchange. Even if we consider the largest possible value for J′ = J/2, the variational energy of the Néel state in Fig. 1(b) is then –(1/2)(N^2/2)J′ = –(1/8)N^2J, while that of the frozen valence bond state in Fig. 1(c) (with N^2/4 singlet bonds) is –(3/4)N^2/4J = –(3/16)N^2J. Thus the frozen valence bond state dominates over the dimer SDW, implying that the dimerization of the dimer lattice is unconditional, and the difference from the simpler $\rho = 1$ case arises from the smaller (by factor of 2) exchange integral in the uniform dimer lattice of Fig. 1(b). The above approach is obviously simplistic, but no more so than the physical argument for the dominance of the SDW in $\rho = 1$.

APPENDIX 2: NUMERICAL METHODOLOGY

A. Contstrained Path Monte Carlo (CPMC)

The CPMC ground-state quantum Monte Carlo method[58] uses a constraining trial wavefunction to eliminate exponential loss of signal due to the Fermion sign problem. Although the method has been thoroughly

bench-marked against known results for the Hubbard model, the method is non-variational, and it is important to check its accuracy in every new system against exact results and to use a variety of different trial wavefunctions. The current application is different from previous ones in including the V interaction, as well as in the choice of the bandfilling (previously tested cases were for bandfillings close to 1/2). Furthermore, previous work has shown that most accurate results are obtained when the trial noninteracting wavefunctions have "closed-shell" nondegenerate configurations. In the next subsection it is shown that the proper boundary conditions for simulating coupled 1/4-filled band chains involves having 4n electrons (where n is an integer) per chain. This implies degeneracy of the trial wavefunctions at $t_\perp = 0$ and again near $t_\perp = 1$. It is thus necessary to check the accuracy of the method for our purpose, and this was done by comparing CPMC results with the exact results for the 8×2 lattice.

Fig. 13 summarizes the results of the bench-mark energy calculations for an 8×2 lattice, periodic in the x-direction, with $U = 6$ and $V = 1$. Both undistorted and and the $2k_F$ ($r_{2k_F} \neq 0, r_{4k_F} = 0$ in Eq. (7)) bond distorted systems were compared, where for the the uniform lattice all hopping integrals were taken to be 1.0, while for the distorted system they were 1.14, 1.0, 0.86 and 1.0 (as in Fig. 2(a)). For this amplitude of the $2k_F$ distortion,

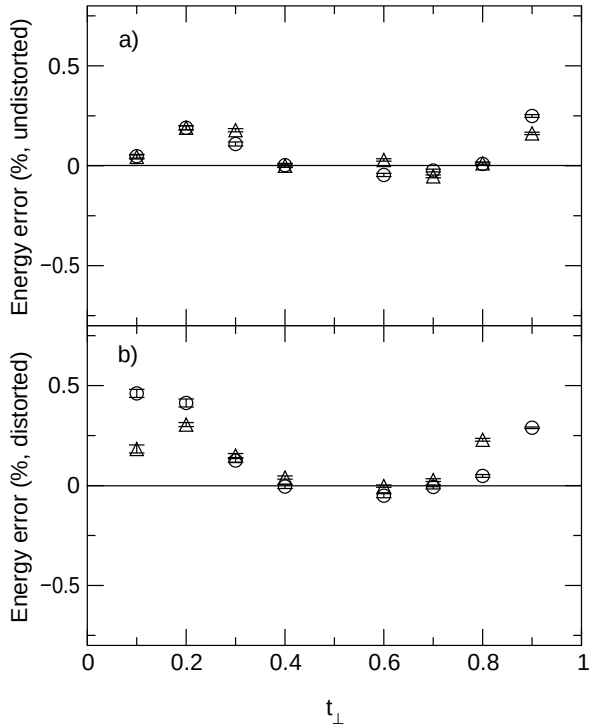

FIG. 13. Percent errors in the CPMC energies for (a) undistorted and (b) $2k_F$ bond-distorted (the hopping integrals in the distorted lattice correspond to those in Fig. 2(a)) 8×2 lattices with $U = 6$ and $V = 1$. Triangles are for the free-electron trial function; circles for the UHF trial function.

the absolute value of ΔE is only 0.3% of the total energy (at $t_\perp = 0.4$). Such a small energy difference is not easy to measure within quantum Monte Carlo. We note that energy differences of this order of magnitude have also been calculated using CPMC to study hole binding in the the 3-band Hubbard model[59]. The CPMC values are scaled for $\Delta\tau \to 0$ from $\Delta\tau = 0.05$ and $\Delta\tau = 0.1$ to remove the Trotter discretization error. The trial wavefunctions used were either the free-electron wavefunction, or an Unrestricted Hartree-Fock (UHF) wavefunction with $U = 2$ and $V = 0.5$. Hartree-Fock wavefunctions with larger U and V gave less accurate results, probably due to the tendency of UHF to exaggerate AFM correlations. In Fig. 13 the UHF trial functions produced larger errors than the free-electron trial functions for the distorted system at small $t_\perp$ because the SDW correlations there are exaggerated by the UHF approximation. The CPMC systematic errors are largest at small $t_\perp$ (< 0.2) and large $t_\perp$ (> 0.8) possibly due to the degeneracies in the one-electron occupancies at $t_\perp = 0$ and $t_\perp = t$. However, at large $t_\perp$, the UHF trial wavefunction produced slightly more accurate results for the 8×2 distorted lattice possibly because the numerically-derived UHF wavefunction breaks some of the symmetry of the non-interacting wavefunction. In the intermediate $t_\perp \sim 0.4$ regime, the CPMC energies are indistinguishable from the exact energies within the statistical error. The accuracy of the CPMC method in this region is very reassuring, since for the *non*interacting case, at $t_\perp = 0.4$ the distortion has already vanished.

In addition to comparing energies, we have also compared charge densities and spin-spin correlation functions. Table I compares the charge densities and spin-spin correlations computed by CPMC for the 8×2 distorted lattice at $t_\perp = 0.4$. The agreement with the exact result is not as good as for the energy (typically 1-5% for the charges and 5-10% for the spin-spin correlations), but is more than adequate to identify the presence and periodicity of the broken symmetry states. Thus in general, we find the CPMC results are close to the exact results

$\langle \rho_j \rangle$			$\langle s_i^z s_j^z \rangle$		
j	exact	CPMC	i,j	exact	CPMC
1	0.4799	0.4756(6)	1,9	-0.06095	-0.0585(7)
2	0.5201	0.5250(6)	1,10	-0.03215	-0.0312(7)
3	0.5201	0.5240(6)	1,11	0.01408	0.0161(7)
4	0.4799	0.4772(6)	1,12	-0.02698	-0.0231(6)
			1,13	-0.07299	-0.0687(6)
			1,14	-0.03085	-0.0268(5)
			1,15	0.01408	0.0158(6)
			1,16	-0.02552	-0.0239(7)

Table I. Comparison of CPMC and exact charge density and spin-spin correlations for an 8×2 system with $U = 6$, $V = 1$, $t_\perp$=0.4, with the same distortion of hopping integrals as in Figure (13). Sites on the first chain are numbered 1 – 8, those on the second chain 9 – 16.

for both energies and correlation functions, except for very small or large $t_\perp$.

B. Boundary Conditions

As noted above, we determine the proper combinations of lattices and boundary conditions for the numerical simulations by the requirement that nonzero $t_\perp$ destabilizes the BCDW for *noninteracting* electrons with those boundary conditions on that particular finite lattice: *i.e.*, we require the finite lattices to reflect correctly the known behavior of the noninteracting case in the thermodynamic limit.

Consider an N × M lattice, with N sites along the chain and M chains. To avoid odd/even effects, consider an even number of electrons per chain. This number can then be either 4n or 4n + 2, where n is an integer. To obtain a 1/4-filled band, one can then have N = 4n × 2 = 8n or N = (4n + 2) × 2= 8n + 4. The proper N for our purpose is N = 8n (*i.e.*, 4n electrons per chain). This follows from the one-electron energy levels of coupled chains with 4n and 4n + 2 electrons per chain. In Fig. 14 below we have shown the one-electron energy levels for the undistorted 8 × 2 (top panel, labeled a) and 12 × 2 (bottom panel, labeled b) lattices (both periodic in the x-direction), corresponding to $t_\perp = 0$ on the left and 0.1 on the right in both cases. In the 8 × 2 lattice, the degeneracy at $t_\perp = 0$ will lead to spontaneous distortion. For nonzero $t_\perp$ and a π-phase shift between chains (which gives lower energy than phase shifts of 0 or $\frac{\pi}{2}$), the pairs of one-electron levels that are coupled by phonons with wave-vector ($2k_F$, π) are ($-\frac{2\pi}{8}$, 0) and ($+\frac{2\pi}{8}$, π); and ($+\frac{2\pi}{8}$, 0) and ($-\frac{2\pi}{8}$, π). The finite gap that occurs for $t_\perp \neq 0$ between each pair of one-electron

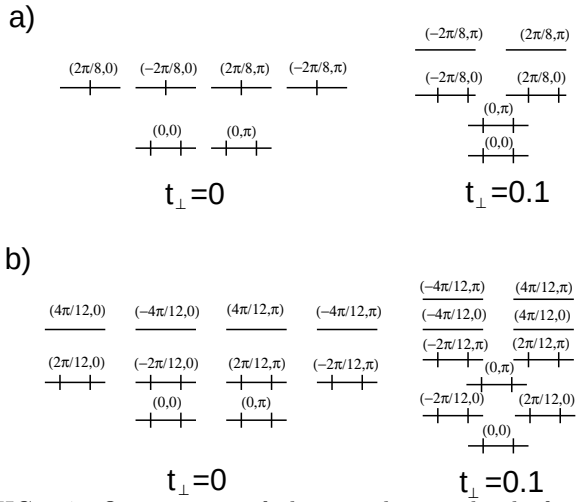

FIG. 14. Occupancies of the one-electron levels for the undistorted (a) 8 × 2 lattice, with $t_\perp = 0$ (left) and $t_\perp = 0.1$ (right) and (b) 12 × 2 lattice, also with $t_\perp = 0$ (left) and $t_\perp = 0.1$ (right).

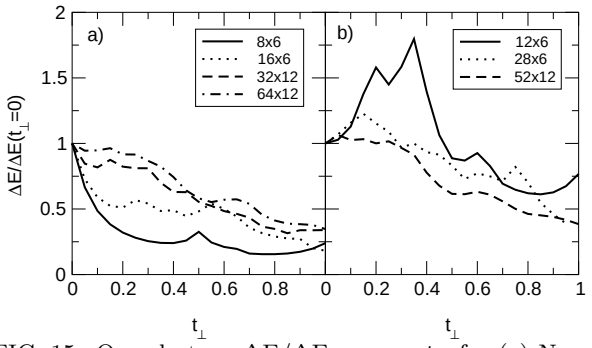

FIG. 15. One-electron $\Delta E/\Delta E_0$ versus $t_\perp$ for (a) N = 8n and (b) N = 8n+4. In each case results for several N × M lattices are shown.

levels coupled by the ($2k_F$, π) phonon indicates absence of nesting and the destabilization of the distortion. This energy gap increases with $t_\perp$, leading to a decrease in ΔE with $t_\perp$ for N = 8n (see Fig. 15 for details), as occurs in the thermodynamic limit. In contrast, consider the 12 × 2 lattice, in which the one-electron ground state is non-degenerate. There is now a nonzero energy gap between the levels coupled by the $2k_F$ electron-phonon interaction already at $t_\perp = 0$ ($k_x = -\frac{2\pi}{12}$ and $k_x = +\frac{4\pi}{12}$; $k_x = +\frac{2\pi}{12}$ and $k_x = -\frac{4\pi}{12}$). With nonzero $t_\perp$, and once again a π-phase shift between the chains, the energy gap between the levels ($-\frac{2\pi}{12}$, π) and ($+\frac{4\pi}{12}$, 0), and similarly that between the levels ($+\frac{2\pi}{12}$, π) and ($-\frac{4\pi}{12}$, 0), *decreases*, indicating that the tendency to distort here *increases with inter-chain coupling*, at least for small to moderate $t_\perp$.

For large N, the difference between N = 8n and N = 8n+4 vanishes, as is shown in Fig. 15, where Figs. 15 (a) and (b) show the behavior of $\Delta E(t_\perp)$ for N = 8n and 8n+4, respectively. The qualitative behavior (destabilization of the distortion) is the same for all N = 8n, and monotonically decreasing ΔE is also seen for N = 8n+4 for large N, but finite size effects (increasing ΔE at small

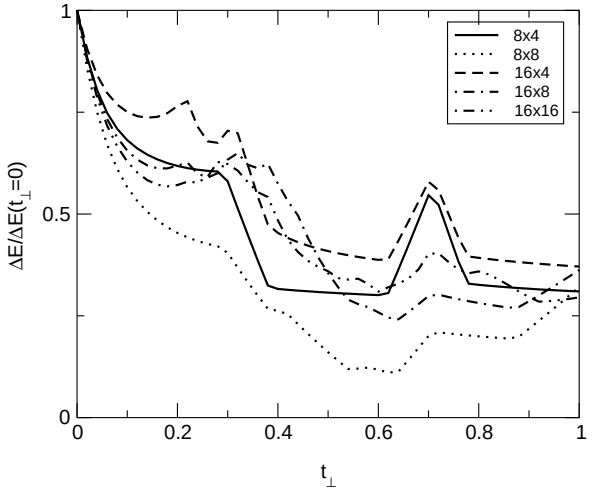

FIG. 16. One-electron $\Delta E/\Delta E_0$ for the 8 × 4, 8 × 8, 16 × 4, 16 × 8 and 16 × 16 lattices for the $2k_F$ bond distortions as in Fig. 2(a).

to intermediate $t_\perp$) are strong even for N = 28, a chain length already too large for accurate 2D many-body calculations. The correct qualitative behavior of all N = 8n is the basis of our choice of these N.

In contrast to the choice of N, there is no immediate restriction on the choice of M, the number of chains, except that M should be even, to avoid even/odd effects. M = 4n and 4n + 2 both show the same qualitative behavior, as seen from the plots of ΔE versus $t_\perp$ in Fig. 16, for several M = 4n lattices (M = 4n + 2 are included in Fig. 15). Thus both M = 4n and 4n + 2 are appropriate. Our choice of M = 4n + 2 is based on two reasons. First, exact diagonalization calculations on the 8×2 lattice allows comparisons to results obtained within CPMC, and the exact diagonalizations cannot be done for the next larger appropriate lattice, viz. 8 × 4. Second, the M = 4n lattices are characterized by one-electron Fermi level degeneracies for $t_\perp \neq 0$ (even though the degenerate levels are not coupled by ($2k_F$, π) phonons), and the absence of a single well-defined one-electron wave-function would make the CPMC calculations considerably more difficult than for M = 4n + 2 lattices, which have non-degenerate one-electron levels for nonzero $t_\perp$.

C. UHF calculations of bond distortion

As discussed in the subsection on methods in this Appendix, UHF trial wavefunctions for the CPMC calculations were constructed for regions where one-electron wavefunctions were degenerate. Since UHF calculations give reasonably correct results in the small U, V range it is also of interest to determine the tendency of the 2D lattice to distort within the UHF approximation. One advantage of this procedure is that much larger lattices than those discussed in section IV can be tested. We report these results here. We have chosen relatively small U and V for two reasons: the UHF procedure does not converge well for larger interactions, and the smaller

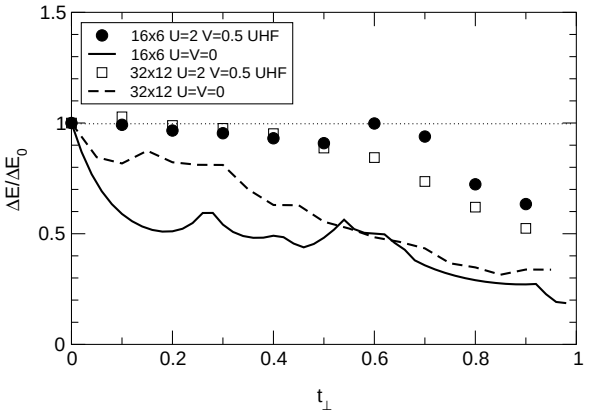

FIG. 17. $\Delta E/\Delta E_0$ versus $t_\perp$ for a $2k_F$ bond distortion ($r_{4k_F} = 0$) for noninteracting and the interacting lattices within the UHF approximation. Intra-chain hopping integrals for the distorted lattices are as indicated in Fig. 2(a).

values of U and V gave better results when used as a CPMC trial function (compared to a numerically exactly solved 8×2 system). Fig. 17 shows the normalized energy gain from a $2k_F$ distortion for two different lattices, within the UHF approximation. The UHF results show that $\Delta E/\Delta E_0$ remains close to 1 for at least up to $t_\perp \sim 0.4$, indicating a tendency to persistent distortion up to this $t_\perp$. Although $\Delta E/\Delta E_0$ begins to decrease at still larger $t_\perp$, these calculations are for a relatively small value of U, and as discussed in section III, the range of $t_\perp$ over which the distortion should persist increases with U. Thus the qualitative effects of the e-e interaction are already visible within the UHF approach at small U, while a fully persistent broken symmetry state will occur only for larger values of the e-e interaction that are beyond the scope of the UHF. Given that the UHF approximation predicts a vanishing of the bond dimerization in the 1/2-filled band for a fairly small U_c (the actual magnitude of U_c depends on α), in contrast to the correct result that there is an enhancement of the dimerization[1] for $0 < U < 4$, the present results, showing a persistence of the distortion for moderate $t_\perp$, is initially perplexing. The reason for the correct prediction in this case is that the UHF exaggerates the SDW, which destroys the BOW in the 1/2-filled band, but has a co-operative interaction with the 1/4-filled band BOW for small to moderate $t_\perp$.

APPENDIX 3: SPIN CHARACTER OF THE GROUND STATE

As discussed in Appendix 2, the proper boundary condition for the numerical evaluation of the electronic energy gained upon bond or site distortion in $\rho = 1/2$ involves finite N × M lattices with N = 8n. This requires the number of electrons per chain to be 4n, and it is known that in 1D periodic *undistorted* rings with $\rho \neq 1$, the ground state has overall spin S = 1 instead of 0 for any nonzero U.

$t_\perp$	undistorted		$2k_F$ distortion	
	S=0	S=1	S=0	S=1
0.01	-9.335651	-9.335637	-9.352522	-9.352228
0.025	-9.337570	-9.336944	-9.354380	-9.353739
0.05	-9.344122	-9.341546	-9.361083	-9.358425

Table II: The S=0 and S=1 energies of the 8×2 undistorted and $2k_F$ bond-distorted lattice for $U = 6$ and $V = 1$. The lowest energy is S=0 for both undistorted and distorted cases.

The spin of the ground state of the distorted periodic ring depends on its size and the magnitude of the Hubbard U. For the values of the correlation parameters and bond distortion parameter in Fig. 4, the ground state in the N = 8 distorted periodic ring has S = 1, while the N = 16 ground state has S = 0. Thus the ΔE_0 in Fig. 4 for nonzero e-e interaction corresponds to ΔE_{TT} (*i.e.*,

the energy gained by the triplet state upon bond distortion) for N = 8, and to ΔE_{TS} (undistorted state in S = 1, distorted state in S = 0) for N = 16. Whether or not the comparisons of the zero and nonzero $t_\perp$ are then meaningful is an important question. We present here the detailed results of three different sets of calculations, each of which indicates that our interpretation of the results of Fig. 4 (viz., strong tendency of the interacting 1/4-filled lattice to distort at arbitrary $t_\perp$) is correct.

First, we have calculated the exact ground states of the 8×2 lattice for $t_\perp$ as small as 0.01. In Table II we have given the S = 0 and S = 1 energies of the 8×2 lattice for $U = 6$ and $V = 1$, for three small values of $t_\perp$. The coupled chain system is in the S = 0 state for *both* zero and nonzero bond distortion for the smallest nonzero $t_\perp$. The important point now is that instead of choosing the single isolated chain as the standard in Fig. 4, we could have also chosen the coupled chain system with $t_\perp = 0.01$ as the standard, provided the distortion of the $t_\perp = 0.01$ lattice is also unconditional. Even if the nesting ideas were valid, we believe that the coupled chain system with $t_\perp = 0.01$ is unconditionally distorted and then the results in Table II clearly show that ΔE increases with further increase in $t_\perp$, indicating enhanced distortion relative to $t_\perp = 0.01$. The error bars in the CPMC calculations prevent us from performing similar calculations for the 8×6 or the 16×6 lattices, but the overall similarities in the (a) occupancies of the one-electron levels for nonzero $t_\perp$ and (b) ΔE behavior, especially in the region $t_\perp \leq 0.4$, preclude different behavior at small nonzero $t_\perp$.

We performed a second set of calculations for the 8×2 lattice for very small values of U (with $V = 0$). Note that if the persistent distortion implied in Fig. 4 were merely due to our choosing the wrong reference point $t_\perp = 0$

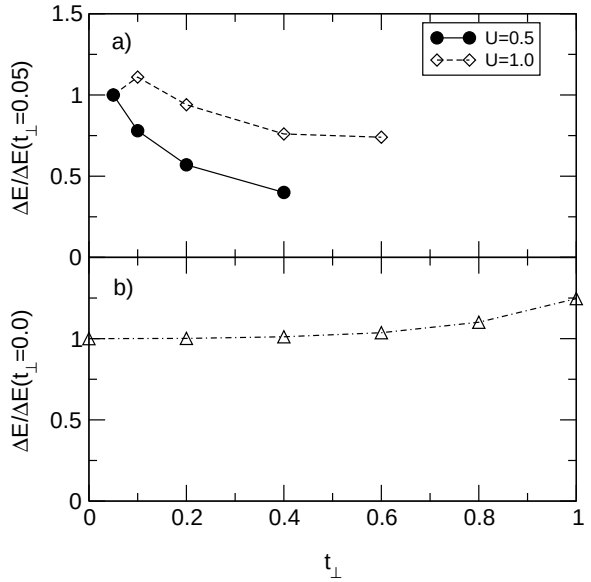

FIG. 18. (a) ΔE *vs.* $t_\perp$ for the 8×2 lattice at small U (normalized to the value at $t_\perp = 0.05$). Note the decrease in the ΔE. (b)$\Delta E/\Delta E_0$ *vs.* $t_\perp$ for the 8×2 lattice at $U = 100$.

(since exactly at this point $\Delta E_0 = \Delta E_{TT}$), an apparently enhanced distortion for nonzero $t_\perp$ should occur for *all* nonzero U (since the single chain is S = 1 for all nonzero U, while the coupled chain system has S = 0 for all nonzero $t_\perp$ and U). On the other hand, if the results in Fig. 4 are due to the confinement effect discussed in section III.D, then enhanced/persistent distortion should occur only *above a threshold e-e interaction*: for weak e-e interaction the behavior should resemble that of the non-interacting lattice (with enhanced or persistent distortion occurring for a small range of $t_\perp$ near $t_\perp = 0$). We show here the results of calculations at small U for *site* distortion (as opposed to bond distortion), since we also report calculations for very large U below, and the bond distortion pattern (the magnitude of r_{4k_F}) is U-dependent, but the site distortion pattern is not. The distorted lattice here has site energies $+\epsilon$, $+\epsilon$, $-\epsilon$, $-\epsilon$ (with $\epsilon = 0.1$) over four consecutive sites, and a π-phase shift between the two periodic rings. Since the $2k_F$ CDW has a synergetic coexistence with both the $r_{4k_F} = 0$ BOW (Fig. 2(a)) and the $r_{4k_F} \neq 0$ BOW (Fig. 2(b))[27] a persistent CDW also implies persistent BOW; we have confirmed this by calculating the expectation values of the bond orders. In Fig. 18(a) we show the ΔE behavior as a function of $t_\perp$ for both $U = 0.5$ and $U = 1$. Decreasing ΔE with $t_\perp$ is a clear signature that the tendency to distortion here *decreases* with increasing two dimensionality, since confinement at these small U is not sufficient to give persistent distortion. Even though these calculations are with fixed site energies, the expectation values of the charge densities depend on $t_\perp$, and our calculated CDW amplitudes decrease with $t_\perp$, as expected from Fig. 18(a). This behavior is exactly opposite to that in Fig. 5(b), indicating again a decrease in distortion with $t_\perp$ at small U. Finally, we emphasize that similar calculations have also been done with fixed $2k_F$ bond distortion, and once again we observe decreasing ΔE and CDW amplitude with increasing $t_\perp$.

We performed a third set of calculations with very large $U = 100$, again with the same site distorted lattice but now with $\epsilon = 0.2$, since at this very large U, the energy gained upon distortion for $\epsilon = 0.1$ is very small. The resultant BOW here has strong $4k_F$ component ($r_{4k_F} \neq 0$), and this is why the distorted lattice was chosen to be the $2k_F$ CDW in this and the above calculations, such that meaningful comparisons between these extreme cases can be made. At this large U, the energy difference between S = 0 and S = 1 states is negligible. For example, for the 1D 8-site periodic ring ΔE_{SS} (electronic energy gained in the S = 0 subspace, with both undistorted and distorted states in S = 0) = 0.06222, while ΔE_{TT} (electronic energy gained in the S = 1 subspace, with both undistorted and distorted states in S = 1) = 0.06224. Fig. 18(b) shows the ΔE behavior as a function of $t_\perp$ (with $\epsilon = 0.2$ now). An enhanced CDW (and therefore BOW) is seen from as a function of $t_\perp$, where the singlet and triplet data points at $t_\perp = 0$ are the same. As seen in Fig. 18(b), the ΔE for nonzero $t_\perp$ is weakly en-

hanced now even when compared to ΔE_{SS} at $t_\perp = 0$. Once again, the behavior of the CDW amplitude is in complete agreement with the prediction from Fig. 18(b), viz., a weak enhancement of the CDW amplitude with $t_\perp$.

Considering the above three different sets of results, we therefore conclude that the results in Fig. 4, Fig. 5(b) and Fig. 9 are not artifacts, and the persistent distortion is real and a true confinement effect, as would also be expected from the "variational" arguments in Appendix 1.

---

[1] D. Baeriswyl, D.K. Campbell and S. Mazumdar in *Conjugated Conducting Polymers*, edited by H. Kiess (Springer Verlag, Berlin, 1992) pp. 7 - 133.

[2] A.J. Heeger, S. Kivelson, R.J. Schrieffer and W.-P. Su, Rev. Mod. Phys., **60**, 781 (1988).

[3] S.N. Dixit and S. Mazumdar, Phys. Rev. B**29**, 1824 (1984). S. Mazumdar and D.K. Campbell, Phys. Rev. Lett. **55**, 2067 (1985).

[4] S. Kivelson, Phys. Rev. B **28**, 2653 (1983).

[5] W.-P. Su, Solid St. Commun. **48**, 479 (1983).

[6] J.E. Hirsch, Phys. Rev. Lett. **53**, 2327 (1984).

[7] E. Manousakis, Rev. Mod. Phys. **63**, 1 (1991) and references therein.

[8] S. Mazumdar Phys. Rev. B **36**, 7190 (1987) and *ibid*, **39**, 12324 (1989).

[9] F.C. Zhang and P. Prelovsek, Phys. Rev. B **37**, 1569 (1988).

[10] S. Tang and J.E. Hirsch, Phys. Rev. B **37**, 9546 (1988) and *ibid*, 12327 (1989).

[11] A.W. Sandvik, Phys. Rev. Lett. **83**, 3069 (1999).

[12] I. Affleck and B. Halperin, J. Phys. A **29**, 2627 (1996).

[13] Z. Wang, Phys. Rev. Lett. **78**, 126 (1997).

[14] E. Dagotto and T.M. Rice, Science, **271**, 618 (1996) and references therein.

[15] F.D.M. Haldane, Phys. Lett. **93A**, 464 (1983).

[16] J. Solyom, Adv. Phys. **28**, 201 (1979).

[17] V.J. Emery in *Highly Conducting One-Dimensional Solids*, edited by J.T. Devreese et al., (Plenum, N.Y. 1979).

[18] J. Voit, Rep. Progr. Phys. **58**, 977 (1995).

[19] J.E. Hirsch and D.J. Scalapino, Phys. Rev. B **27**, 7169 (1983) and *ibid* **29**, 5554 (1984).

[20] S. Mazumdar, S.N. Dixit and A.N. Bloch, Phys. Rev. B **30**, 4842 (1984).

[21] We exclude from our discussions the extensive work on doped 2- and 4-leg ladder systems. It is not clear currently whether or not these results are relevant for the true 2D lattice.

[22] A true metallic phase may not be obtained because of disorder effects, but this is a different issue that is unrelated to the question of the existence of density waves, and is hence ignored here.

[23] H.H. Lin, L. Balents and M.P.A. Fisher, Phys. Rev. B **56**, 6569 (1997).

[24] S. Mazumdar, S. Ramasesha, R. Torsten Clay and D.K. Campbell, Phys. Rev. Lett. **82**, 1522 (1999).

[25] An abbreviated discussion of the evolution of the BCSDW into the BCDW for large $t_\perp$ can be found in S. Mazumdar, R. T. Clay, and D. K. Campbell, cond-mat/9910164.

[26] K.C. Ung, S. Mazumdar and D.K. Campbell, Solid St. Commun. **85**, 917 (1993).

[27] K.C. Ung, S. Mazumdar and D. Toussaint, Phys. Rev. Lett. **73**, 2603 (1994).

[28] J. Riera and D. Poilblanc, Phys. Rev. B **59**, 2667 (1999).

[29] T. Holstein, Ann. Phys. **8**, 325 (1959).

[30] D. Jerome and H. Schulz, Adv. in Phys. **31**, 299 (1982).

[31] T. Ishiguro, K. Yamaji and G. Saito, *Organic Superconductors*, 2nd Ed., Springer Series in Solid State Sciences, Vol. 88 (Springer Verlag, Berlin, 1998).

[32] D. Jerome, Science **252**, 1509 (1991).

[33] P.W. Anderson, Phys. Rev. Lett. **67**, 3844 (1991).

[34] D.G. Clarke, S.P. Strong and P.W. Anderson, Phys. Rev. Lett. **73**, 1007 (1994).

[35] Given that the issue of confinement in interacting electron systems has been hotly debated, it is pertinent to emphasize that we use this expression in a considerably narrower sense than has sometimes been used in the literature. Our interest lies strictly in the interacting 1/4-filled band case, and it is not being implied that the effect discussed here applies to other bandfillings.

[36] J.P. Pouget and S. Ravy, J. Physique I, **6**, 1501 (1996).

[37] C. Bourbonnais, Synth. Metals **84**, 19 (1997).

[38] K. Kanoda, Hyperfine Interactions, **104**, 235 (1997).

[39] H. Kino and H. Fukuyama, J. Phys. Soc. Jpn. **65**, 2158 (1996).

[40] R.H. McKenzie, Comments Cond. Mat. Phys. **18**, 309 (1998).

[41] P.M. Chaikin, J. Phys. I. (France) **6**, 1875 (1996).

[42] L.P. Gor'kov, J. Phys. I. (France) **6**, 1697 (1996).

[43] In all cases X are inorganic anions that play only indirect roles in accepting electrons from the organic cations, and do not have any active role in charge transport, although they do influence the magnitudes of the interchain hopping integrals.

[44] J.P. Pouget and S. Ravy, Synth. Metals, **85**, 1523 (1997).

[45] S. Kagoshima, Y. Saso, M. Maesato, R. Kondo and T. Hasegawa, Solid St. Commun. **110**, 479 (1999).

[46] The BCSDW has also been found in 1D Hartree-Fock calculations within the dimerized dimer lattice, see N. Kobayashi and M. Ogata, J. Phys. Soc. Jpn. **66** 3356 (1997). The SDW component here, however, is an artifact of the Hartree-Fock approximation as in 1D the spin couplings are necessarily singlet.

[47] The underlying $x \leftrightarrow y$ symmetry in the isotropic 2D limit implies that there are two degenerate orthogonal 2D BCDW states for $t_\perp = t$.

[48] R. T. Clay, A. W. Sandvik, and D. K. Campbell, Phys. Rev. B **59**, 4665 (1999).

[49] M. Nakamura, cond-mat/9909277.

[50] J. Hubbard, Phys. Rev. B **17**, 494 (1978).

[51] Note that Hartree-Fock calculations will predict this ...1010...ordering for *any non-zero* V, and indeed will predict the n-dimensional generalization of this order for an n-

dimensional hypercubic lattice. This artifact of the mean-field approach is known rigorously to be incorrect in 1D and is shown by our later results to be incorrect in 2D. Only in the limit $U >> V >> t$ does this "checkerboard" order actually become the dominant broken symmetry.
[52] D.J. Klein and W.A. Seitz, Phys. Rev. B **10**, 3217 (1974).
[53] P. Jordan and E. Wigner, Z. Phys. **47**, 631 (1928).
[54] J.D. Johnson and B. McCoy, Phys. Rev. A **6**, 1613 (1972).
[55] H. Q. Lin, E. R. Gagliano, D. K. Campbell, E. H. Fradkin, and J. E. Gubernatis, in *The Hubbard Model*, edited by D. Baeriswyl *et al.* (Plenum Press, New York, 1995), pp. 316 – 336.
[56] F.D.M. Haldane, Phys. Rev. Lett. **45**, 1358 (1980); J. Phys. C **14**, 2585 (1981).
[57] K. Moulopoulos and N. Ashcroft, Phys. Rev. B **48** 11646 (1993).
[58] S. Zhang, J. Carlson and J.E. Gubernatis, Phys. Rev. Lett. **74**, 3652 (1995); Phys. Rev. B **55**, 7464 (1997).
[59] M. Guerrero, J.E. Gubernatis and S. Zhang, Phys. Rev. B **57**, 11980 (1998).
[60] S. Mazumdar, D. Campbell, R.T. Clay and S. Ramasesha, Phys. Rev. Lett. **82**, 2411 (1999).
[61] K. Yamaji, J. Phys. Soc. Jpn. **55**, 860 (1986).
[62] B. Domoulin, C. Bourbonnais, S. Ravy, J.P. Pouget and C. Coulon, Phys. Rev. Lett. **76**, 1360 (1996).
[63] D.S. Chow, F. Zamborzsky, B. Alavi, D.J. Tantillo, A. Baur, C.A. Merlic and S.E. Brown, cond-mat/0004106.
[64] H.J. Schulz in *Low Dimensional Conductors and Superconductors*, edited by D. Jerome and L.G. Caron (Plenum, N.Y. 1987), pp. 95 – 112.
[65] C. Coulon, P. Delhaes, S. Flandrois, R. Lagnier, E. Bonjour, J.M. Fabre, J. Physique **43**, 1059 (1982).
[66] S.S.P. Parkin, J.C. Scott, J.B. Torrance and E.M. Engler, J. Physique Colloque, **44**, C-3, 1111 (1983).
[67] In order to explain the "purely electronic CDW", Kobayashi et al., in a 1D calculation have suggested that the transition to the ...1100... CDW is driven by a second neighbor intra-chain Coulomb interaction V_2 [N. Kobayashi et al., J. Phys. Soc. Jpn. **67**, 1098 (1998)]. The synergic coexistence of the BOW and the CDW found by us indicates that a BOW must exist even in this case.
[68] G. Grüner, Rev. Mod. Phys. **66**, 1 (1994) and references therein.
[69] T. Sasaki and N. Toyota, Synth. Metals, **70**, 849 (1995).
[70] F.L. Pratt, T. Sasaki, N. Toyota and K. Nagamine, Phys. Rev. Lett. **74**, 3892 (1995).
[71] P. Wzietek, F. Creuzet, C. Bourbonnais, D. Jerome, K. Bechgaard and P. Batail, J. Physique I **3**, 171 (1993).
[72] K. Miyagawa, A. Kawamoto, Y. Nakazawa and K. Kanoda, Phys. Rev. Lett. **75**, 1174 (1995).
[73] K. Miyagawa, A. Kawamoto and K. Kanoda, Phys. Rev. B **56**, R8487 (1997).
[74] N. Harrison, Phys. Rev. Lett. **83**, 1395 (1999).
[75] N. Biskup, J.A.A.J. Perenboom, J.S. Brooks and J.S. Qualls, Solid St. Commun. **107**, 503 (1998).
[76] P.L. Kuhns, J.S. Brooks, T. Caldwell, W.G. Moulton, A.P. Reyes, N. Biskup, A.M. Kini, J.A. Schlueter, H.H. Wang, U. Geiser and J.M. Williams, Solid St. Commun. **109**, 637 (1999).
[77] H. Mori, S. Tanaka, M. Oshima, G. Saito, T. Mori, Y. Maruyama, and H. Inokuchi, Bull. Chem. Soc. Jpn. **63**, 2183 (1990).
[78] L. Ducasse and A. Fritsch, Solid St. Commun. **91**, 201 (1994).
[79] H. Seo, cond-mat/9911329.
[80] H. Mayaffre, P. Wzietek, D. Jerome, C. Lenoir and P. Batail, Phys. Rev. Lett. **75**, 4122 (1995).
[81] A. Kawamoto, K. Miyagawa, Y. Nakazawa and K. Kanoda, Phys. Rev. Lett. **74**, 3455 (1995).
[82] Y. Nakazawa and K. Kanoda, Phys. Rev. B **60**, 4263 (1999).
[83] T. Komatsu, N. Matsukawa, T. Inoue, and G. Saito, J. Phys. Soc. Jpn. **65**, 1340 (1996).
[84] H. Kobayashi, T. Udagawa, H. Tomita, K. Bun, T. Naito and A. Kobayashi, Chem. Lett., 1559 (1993).
[85] H. Tanaka, A. Kobayashi, T. Saito, K. Kawano, T. Naito and H. Kobayashi, Adv. Mater. **8**, 812 (1996).
[86] L.K. Montgomery, T. Burgin, J.C. Huffman, J. Ren, and M.-H. Whangbo, Physics C **219**, 490 (1994).
[87] H. Kobayashi, H. Akutsu, E. Arai, H. Tanaka and A. Kobayashi, Phys. Rev. B **56**, R8526 (1997).
[88] H. Seo and H. Fukuyama, J. Phys. Soc. Jpn. **66**, 3352 (1997).
[89] N. Katoh and M. Imada, J. Phys. Soc. Jpn. **63**, 4529 (1994); ibid, **64**, 1437 (1995).
[90] A. Schwartz, M. Dressel, G. Grüner, V. Vescoli, L. Degiorgi and T. Giamarchi, Phys. Rev. B **58**, 1261, (1998).
[91] V. Vescoli, L. Degiorgi, W. Henderson, G. Grüner, K.P. Starkey and L.K. Montgomery, Science **281** 1181 (1998).
[92] S. Mazumdar, in *Interacting Electrons in Reduced Dimensions*, eds. D. Baeriswyl and D.K. Campbell, NATO ASI Series B, Vol. 213 (Plenum, NY, 1989), pp. 315 - 329.
[93] R.L. Greene in *Organic Superconductivity*, eds. V. Kresin and W.A. Little, Plenum, N.Y. (1990), pp. 7 – 13.
[94] Y.J. Uemura, L.P. Le, G.M. Luke, B.J. Sternlieb, J.H. Brewer, T.M. Riseman, G. Saito and H. Yamochi, in reference 89, pp. 23 – 29.
[95] B. Brandow, Phys. Rep. **296**, 1 (1998).
[96] H. Kondo and T. Moriya, J. Phys. Condens. Matter **11**, L363 (1999).
[97] H. Kino and H. Kontani, J. Phys. Soc. Jpn., **67**, 3691 (1998).
[98] J. Schmalian, Phys. Rev. Lett. **81**, 4232 (1998).
[99] M. Vojta and E. Dagotto, Phys. Rev. B **59**, R713 (1999).
[100] K. Kuroki and H. Aoki, Phys. Rev. B **60**, 3060 (1999).
[101] S. Zhang, J. Carlson and J.E. Gubernatis, Phys. Rev. Lett. **78**, 4486 (1997).
[102] M. Guerrero, G. Ortiz and J.E. Gubernatis, Phys. Rev. B **59**, 1706 (1999).
[103] C.T. Shih, Y.C. Chen, H.Q. Lin and T.K. Lee, Phys. Rev. Lett. **81**, 1294 (1998).
[104] E. Dagotto, Rev. Mod. Phys. **66**, 763 (1994).
[105] D.J. Scalapino, Phys. Rep. **250**, 330 (1995). See also, J. Low Temp. Phys. **117**, 179 (1999).
[106] G.V. Chester, Phys. Rev. A **2**, 256 (1970).
[107] A.F. Andreev in *Progress in Low Temperature Physics,* edited by D.G. Brewer (North Holland, Amsterdam, 1982), Vol. VIII.
[108] D. Nelson and M.E. Fisher, Phys. Rev. Lett. **32**, 1350 (1974).

[109] A.J. Leggett, Phys. Rev. Lett. **25**, 1543 (1970).
[110] A.S. Alexandrov and J. Ranninger, Phys. Rev. B **23**, 1796 (1981); S. Robaskiewicz, R. Micnas and K.A. Chao, Phys. Rev. B **23**, 1447 (1981). Note that these two papers deal with the negative U Hubbard model, which leads to superconductivity via a Bose condensation of small bipolarons. As noted in Ref. 111, this mechanism is unlikely to apply to the high temperature superconductors. We stress that the effective "negative U, positive V" model we envisage here is quite different from the standard "negative U" model in that any bipolarons are expected to be quite extended and thus substantially more mobile. See Refs. 112 for more details. Clearly this issue requires further study.
[111] B.K. Chakraverty, J. Ranninger and D. Feinberg, Phys. Rev. Lett. **81**, 433 (1998).
[112] S. Aubry, p. 217 in *Polarons and Bipolarons in High-T_c Superconductors and Related Materials*, edited by E. K. H. Salje, A. S. Alexandrov, and W. Y. Liang (Cambridge University Press, Cambridge, 1995); L. Proville and S. Aubry, Eur. Phys. J. B **11**, 41 (1999); L. Proville and S. Aubry, Eur. Phys. J. B (to appear).
[113] M. Imada, J. Phys. Soc. Jpn. **60**, 1877 (1991); Phys. Rev. B **48** 550 (1993). Note that in the effective spin-Peierls model related to our incommensurate BCDW state, we do not expect nearest neighbor occupancy of defect pairs, as the weak confinement effects arising from the distorted lattice will allow spatially extended paired states.
[114] V.J. Emery, E. Fradkin and S. Kivelson, cond-mat/0001077.
[115] M.J. Rice and E.J. Mele, Phys. Rev. B **25**, 1339 (1982).
[116] S.C. Zhang, S. Kivelson and A.S. Goldhaber, Phys. Rev. Lett. **58**, 2134 (1987).
[117] R.T. Clay, S. Mazumdar and D.K. Campbell, unpublished.
[118] S.A. Kivelson, V.J. Emery and H.Q. Lin, Phys. Rev. B **42**, 6523 (1990).
[119] S.M. De Soto, C.P. Slichter, A.M. Kini, H.H. Wang, U. Geiser and J.M. Williams, Phys. Rev. B **52**, 10364 (1995).
[120] Y. Nakazawa and K. Kanoda, Phys. Rev B **55**, R8670 (1997).
[121] S. Belin, K. Behnia and A. Deluzet, Phys. Rev. Lett. **81**, 4728 (1998).
[122] J.M. Schrama, E. Rzepniewski, R.S. Edwards, J. Singleton, A. Ardavan, M. Kurmoo and P. Day, Phys. Rev. Lett. **83**, 3041 (1999).
[123] I.J. Lee, M.J. Naughton, G.M. Danner and P.M. Chaikin, Phys. Rev. Lett. **78**, 3555 (1997).
[124] I.J. Lee, D.S. Chow, W.G. Clark, J. Strouse, M.J. Naughton, P.M. Chaikin and S.E. Brown, cond-mat/0001332.